magnetochemistry

MDPI

Review

Iron Oxide Nanoparticles Enabled Ultrasound-Guided Theranostic Systems

Thiago Tiburcio Vicente [1], Prabu Periyathambi [1], Ariane Franson Sanches [1], Marina Yuki Azevedo Nakakubo [1], Nicholas Zufelato [1], Karina Bezerra Salomão [2], María Sol Brassesco [3], Theo Zeferino Pavan [1], Koiti Araki [4] and Antônio A. O. Carneiro [1,*]

[1] Department of Physics, Faculty of Philosophy, Sciences and Letters, University of São Paulo, Ribeirão Preto 14040-900, SP, Brazil; thiagotiburcio37@usp.br (T.T.V.); prabubiochemi87@gmail.com (P.P.); ane_sanches@usp.br (A.F.S.); marina.yuki@usp.br (M.Y.A.N.); theozp@usp.br (T.Z.P.)
[2] Brazilian Biosciences National Laboratory (LNBio), Brazilian Center for Research in Energy and Materials (CNPEM), Campinas 13083-970, SP, Brazil
[3] Department of Biology, Faculty of Philosophy, Sciences and Letters, University of São Paulo, Ribeirão Preto 14040-900, SP, Brazil; solbrassesco@usp.br
[4] Department of Chemistry, Institute of Chemistry, University of São Paulo, Av. Lineu Prestes 748, Butantan, Sao Paulo 05508-000, SP, Brazil
* Correspondence: adilton@usp.br

Abstract

The tumor microenvironment, characterized by higher acidity, hypoxia, and dense cellular structures, plays a pivotal role in cancer progression, therapeutic resistance, and treatment response. Nanoparticle-based contrast agents enable the precise delineation of solid regions within heterogeneous tumors through advanced molecular imaging techniques. Since 1956, ultrasound (US) medical imaging has provided essential anatomical and functional insights about internal organs. More recently, magnetomotive ultrasound (MMUS) has emerged as a promising imaging modality, using a modulated magnetic field to exert force on superparamagnetic iron oxide nanoparticles (SPIONs), inducing motion in the surrounding tissues through mechanical coupling. In parallel, magnetic hyperthermia (MH), which employs localized heating by alternating magnetic fields, has demonstrated significant potential in selectively destroying cancer cells while sparing healthy tissues. This review summarizes the current state of IONP-based contrast agents, with particular emphasis on their use in MH for cancer treatment, as well as their potential in multimodal imaging, including MMUS, and photoacoustic (PA) imaging. The advantages and limitations of IONPs in tumor detection and characterization are discussed, examining the development of surface-functionalized MNPs, and analyzing how material properties and environmental factors affect their diagnostic and therapeutical performance. Finally, strategies for combining MMUS and PA modalities for pre-clinical cancer imaging are proposed.

Keywords: magnetic nanoparticles; magnetomotive ultrasound; photoacoustic imaging; magnetic hyperthermia

Check for updates

Academic Editor: Carlos J. Gómez García

Received: 29 December 2025
Revised: 25 January 2026
Accepted: 30 January 2026
Published: 3 February 2026

Copyright: © 2026 by the authors. Licensee MDPI, Basel, Switzerland. This article is an open access article distributed under the terms and conditions of the Creative Commons Attribution (CC BY) license.

1. Introduction

1.1. Clinical Challenges Motivating Cancer Theranostic Platforms

Cancer is defined as a disease that is associated with abnormal cell growth and uncontrollable cell division that tends to impinge on other tissues in the body by different mechanisms of metastasis [1]. According to the World Health Organization (WHO) and the

International Agency for Research on Cancer (IARC), there were approximately 20 million new cases of cancer, causing 9.74 million deaths worldwide in 2022 [2–4]. The annualized number of new cancer cases by 2040 is projected to reach 29.9 million, while the number of cancer-related deaths will rise to 15.3 million [5–7].

The current traditional cancer diagnostics include biopsy, X-ray imaging (Computed Tomography (CT)), PET (Positron Emission Tomography), MRI (Magnetic Resonance Imaging), US (ultrasound), and blood tests. The choice among those techniques for a specific case depends on the tumor and the type of affected tissues/organs. However, in theranostic applications, where diagnostic and therapeutic functionalities are integrated into a single platform, this approach allows for combined disease detection, real-time monitoring, and therapy, thus increasing diagnostic accuracy and therapeutic efficacy while supporting personalized strategies, thus overcoming the main limitations of conventional approaches, in which diagnosis and treatment are performed separately. Nevertheless, these techniques still face some limitations [8–11]. First, the diagnostic modality must allow rapid data/image acquisition, enabling real-time imaging or assessment immediately before and after treatment. Second, the imaging approach should not interfere with or disrupt the therapeutic procedure. Finally, the availability of low-cost equipment is critical, as it facilitates broader clinical adoption, particularly in developing countries and among low-income populations [12].

Theranostics are not intended to replace well-established medical approaches for tumor detection and classification but rather to enhance treatment delivery by enabling rapid assessment with therapeutic precision and efficacy [13]. In this context, and considering the requirements outlined above, several imaging modalities present distinct advantages and limitations. Nuclear medicine has experienced rapid progress in theranostics, particularly through the development of radiolabeled agents that enable highly sensitive tumor targeting and simultaneous diagnosis and therapy [14,15]. However, ionizing radiation-based techniques raise concerns regarding cumulative radiation dose, logistical complexity, and repeated use during treatment and monitoring. MRI, despite its excellent soft-tissue contrast, relies on complex and high-cost infrastructure and cannot be easily integrated with magnetic or metallic devices commonly used in therapeutic applications. US, in contrast, stands out as a low-cost, real-time, and non-ionizing imaging modality, making it particularly suitable for integration into theranostic platforms.

In this context, the development of multifunctional nanomaterials capable of simultaneously meeting diagnostic and therapeutic demands has emerged as a central strategy in cancer theranostics. Inorganic materials such as iron oxide nanoparticles (IONPs), especially magnetite (Fe_3O_4) and maghemite (γ-Fe_2O_3), stand out among inorganic nanomaterials due to their unique combination of superparamagnetism, high specific surface area, and the possibility of fine-tuning size, shape, and composition, resulting in magnetic, electrical, and optical properties that are not manifested in macroscopic material due to quantum size effects [16,17]. When their dimensions are reduced below about 49 nm, the IONPs exhibit strong superparamagnetic behavior, essential characteristics for safe applications in MRI, magneto hyperthermia (MH), and controlled drug delivery systems [16,18,19]. Furthermore, the high surface reactivity and amphoteric character allow for broad chemical functionalization, including polymeric or lipid coating and conjugation with biological ligands, increasing colloidal stability, biocompatibility, and target specificity, while critically influencing structure-dependent biodistribution and elimination profiles, as highlighted in recent biosafety studies [20–22]. Finally, the endogenous nature of iron, metabolized through established physiological pathways, coupled with the low systemic toxicity and intrinsic biodegradability of IONPs, significantly increases their potential for clinical translation. These attributes distinguish IONPs from other magnetic alternatives, such as cobalt

or nickel ferrites, justifying the widespread preference for the use of IONPs in clinical settings and approval by regulatory agencies such as the Food and Drug Administration (FDA), consolidating them as particularly attractive platforms for diagnostic, therapeutic, and theranostic applications in oncology, central nervous system disorders, and advanced biosensing systems [21,23].

This review provides a comprehensive overview of recent advances in magnetic nanomaterial-based US techniques, with particular emphasis on Magnetomotive Ultrasound (MMUS) and photoacoustic (PA) imaging for cancer diagnosis. It highlights the various mechanisms and engineering strategies employed in the design of IONPs, emphasizing how surface functionalization and structural properties can be adjusted to enhance their imaging and therapeutic capabilities. The objective of this review is, therefore, to advance understanding for the development and application of smart IONPs, which enable multifunctional performance in diagnostic and therapeutic settings. Furthermore, the review discusses the integration of MH with other imaging modalities, including MMUS, PA, and multimodal approaches, highlighting the potential of combining these technologies to improve treatment precision, monitoring, and overall theranostic outcomes. In this framework, US acts as the strategic real-time imaging and monitoring modality, while magnetic and optical interactions are leveraged to introduce molecular specificity, mechanical actuation, and therapeutic control [8–10,24–26].

1.2. Overview of IONPs Applied to Cancer

IONPs are widely studied for application in diagnostics and therapy, especially in cancer treatment, due to their unique properties. Smart IONPs refer to iron oxide nanoparticles that can be prepared to have different shapes and morphologies, such as nanospheres [27–30], nanocubes [31–35], nanoflowers [36], and nanorods [37–40], with specific functionalities provided by their coatings. Examples of organic and inorganic structures commonly used as coatings are polyethylene glycol (PEG) [41,42], chitosan [43], gelatine [44], and bovine and human serum albumin (BSA and HSA) [45,46], as well as noble metals [47], silica [48], Natural Rubber Latex (NRL) [49] and metal oxides, to improve their targeting, drug delivery, imaging and therapeutic capabilities [41,50–54].

IONPs have already received approval from the FDA for clinical use, especially as contrast agents in MRI (e.g., Feridex®, Endorem®, and GastroMARK®), in addition to being incorporated into formulations used in iron replacement therapies [55,56]. Recent studies demonstrate that these NPs also play a relevant role in immunotherapy, acting as immunomodulatory agents capable of interacting with cells of the innate immune system, especially macrophages, influencing their polarization and functional response [57]. IONPs have emerged as tools for biomedical targeting, due to their magnetic properties and biocompatibility. Their application is particularly prominent in cancer therapy, where they can be targeted to tumor sites through the use of external magnetic fields, thus increasing the accuracy of drug delivery, imaging and therapeutic techniques [58–62].

Drug delivery refers to the method or system by which a drug is administered and transported to its site of action in the body [63]. IONP systems can function as magnetic nanocarriers for drug delivery. To this purpose, their surfaces need to be functionalized with different biocompatible materials, such as PEG [64–66], chitosan [67,68], dextran [69], bovine or human serum albumin (BSA and HSA) [45,46,70], gold, and silica [71], for example. These coatings enable interactions or binding with pharmaceutically active compounds, making IONPs highly useful for biomedical applications, particularly in cancer treatments [72]. Recent research has also produced IONPs using different coatings, combined with commonly administered anticancer agents, such as Doxorubicin (DOX) [73–75], Mitoxantrone (MTX) [76–79], Paclitaxel [70,80–82], and Cisplatin [81,83].

Due to their magnetic properties and different formats, IONPs have been used in biomedical imaging techniques such as MRI, Magnetic Particle Imaging (MPI), MMUS and PA imaging. MRI is a non-invasive medical imaging technique that uses magnetic fields and radio waves to generate detailed images of organs and tissues [84]. Unlike methods such as radiography or computed tomography (CT), MRI does not use ionizing radiation, which makes it a safer alternative, especially in situations that require repeated examinations [85]. IONPs are strong enhancers of proton spin–spin relaxation (T2/T2*) and contrast agents for MRI, allowing an enhanced visualization of regions that, under normal conditions, would be difficult to observe accurately [86,87]. This increase in contrast significantly improves MRI's ability to detect diseases at early stages, such as neoplasms [88–90] and neurological disorders [90–92], as well as facilitating a more precise monitoring of the response to treatments [87]. Another imaging technique that plays an important role in pre-clinical and clinical research is Magnetic Particle Imaging (MPI). MPI is an advanced imaging modality that directly detects the nonlinear magnetic response of IONPs, which serve as imaging tracers, providing images with exceptional sensitivity and specificity [93,94]. This technique allows a precise quantification of the concentration and distribution of IONPs in solid tumors and is especially effective in planning hyperthermia-based therapies. Unlike MRI, which detects IONPs indirectly, MPI allows a direct visualization of the biodistribution of these NPs, resulting in highly accurate images that help to optimize therapeutic strategies [95–97]. In addition, MPI has been widely investigated in various biomedical applications, including cardiovascular diagnosis [98–100], neuroimaging [101–103], and tumor detection [93], as well as cell tracking and monitoring [100,104–106].

Both modalities share significant limitations, as they require large, complex equipment and are costly. These limitations have motivated the development of alternative imaging strategies that preserve sensitivity to magnetic nanomaterials while offering greater portability, lower cost, and real-time capabilities. In this context, MMUS has emerged as a promising technique for imaging and tracking IONPs. In MMUS, external magnetic fields are applied to induce motion in tissues containing IONPs, enabling the visualization of their location and dynamics [24,25]. MMUS offers the potential for real-time imaging with high contrast by detecting magnetically induced displacements of IONPs, whose resulting motion is tracked using ultrasound images, enabling precise localization within the target tissue [24,107]. Moreover, MMUS allows monitoring during IONP-guided therapeutic procedures, such as magnetic hyperthermia or targeted therapy, while remaining compatible with conventional ultrasound systems and relatively affordable in terms of cost and potential clinical implementation [108]. This technique has been investigated in various applications, such as the detection of IONPs in the stomach of a rat [109], in mouse tumors and rat lymph nodes [110], as well as in in vivo MMUS imaging in the targeting structure of magnetic drugs based on NPs [111] and the observation of magnetic nanoparticle (MNP) endocytosis by living cells [112].

Complementary to MMUS, PA imaging represents another emerging modality that utilizes the intrinsic properties of IONPs. Due to their strong optical absorption, efficient photothermal conversion, and magnetic responsiveness, IONPs have been widely exploited as contrast agents in photoacoustic imaging [26,113]. PA imaging is a hybrid modality that combines the high contrast of optical imaging with the high spatial resolution of US imaging [26,113,114]. This approach makes it possible to obtain functional images in real time, without the need for ionizing radiation, offering advantages such as greater versatility and better cost–benefit [115].

Finally, these IONPs can also be used in therapeutic techniques such as MH and photothermal therapy (PTT). MH is an alternative therapeutic approach for treating

cancer [116,117]. This technique uses IONPs to generate localized heat when exposed to alternating magnetic fields. This heat is used to increase the temperature of cancer cells to 42–45 °C, resulting in their necrosis without damaging the surrounding healthy tissue [118–121]. When combined with radiotherapy, MH acts synergistically by increasing tumor oxygenation, inhibiting DNA repair mechanisms, and sensitizing tumor cells to ionizing radiation, resulting in greater therapeutic efficacy [122,123]. Similarly, its association with chemotherapy can potentiate the cytotoxicity of drugs, either by increasing cell permeability, through controlled thermal release of drugs, or by overcoming tumor resistance mechanisms [124,125].

Another promising minimally invasive technique for cancer treatment is PTT [126]. This technique uses photothermal agents that can convert near-infrared (NIR) radiation, from 650 nm to 1024 nm, into heat, promoting the selective ablation of malignant tissue in a non-invasive manner. The process involves the localized heating of the target tissue to temperatures above 42 °C, while the surrounding tissue maintains its normal temperature, minimizing collateral damage and preserving healthy structures [126]. The combination of PTT with IONPs can significantly amplify their effectiveness in eliminating cancer cells. This effect is even more pronounced when IONPs are combined with inorganic materials, such as gold [127–129], or functionalized with chemotherapy agents, resulting in a synergistic therapeutic approach [116,130].

Table 1 provides a concise overview of representative studies using IONPs, focused on the techniques described in this subsection, including multimodal implementations, highlighting the composition, size, morphology, surface functionalization, magnetic properties, and key results of NP administration.

Table 1. Key studies using IONPs for diagnosis and therapy, summarizing the properties and the main conclusions.

Application/ Modality	Composition	Size/Shape/ Surface Coating	Magnetic Properties	Main Outcome	References
MMUS and MMUS-SWE/ PA and MMPA Imaging	Fe_3O_4	10–100 nm. Spherical and Gold nanorods Dextran, PEG, Silica, Gold, Citrate, NRL.	Superparamagnetic. High Susceptibility. Strong Magnetic Force Response.	Magnetically induced displacement. Elasticity and viscoelasticity mapping. Detection and localization of sentinel lymph nodes in preclinical and human tissues. Improved PA contrast and optical–thermal conversion.	[24,109,110,131–147]
SPECT/MRI/PET	Fe_3O_4	20–40 nm. Spherical. Dextran, PEG.	Superparamagnetic. High Relaxivity. Magnetic Responsiveness.	Multimodal anatomical. Molecular imaging.	[31–34,36,38,39,72,87, 95,96,134,148]
HM/PTT	Fe_3O_4	10–30 nm. Spherical. Silica, Citrate, Polymer, Proteins, Zinc.	High SAR, Néel/Brownian Relaxation. Optimized Hysteresis Losses.	Localized tumor heating. Real-time localization and thermal dose monitoring.	[36,97,117,119,121, 124,125,143,149–157]
Drug Delivery and Ultrasound-Mediated Therapy	Fe_3O_4-based Hybrid Nanocarriers	30–100 nm. Spherical, Nanocarriers, Nanoclusters. Liposomes, PEG, Chitosan, Graphene, Cell Membrane.	Magnetic Targeting. Dual Magnetic/Thermal Response. Magnetic Steering.	On-demand drug release induced by ultrasound. Synergistic chemotherapy and thermal ablation. Enhanced BBB crossing and glioblastoma treatment.	[9,38,43,46,58,64,67, 73,91,155,158–162]

In this review, "smart" IONPs are defined as nanostructures capable of responding to external or internal stimuli, including magnetic fields, ultrasound, optical excitation, pH variations, or enzymatic activity, thus enabling adaptive diagnostic contrast, targeted therapeutic action, and real-time feedback during treatment. Among these stimuli, ultrasound-based approaches deserve special attention due to their unique combination of real-time operation, absence of ionizing radiation, high temporal resolution, portability, and cost-effectiveness, which together support their integration into bedside and point-of-care clinical workflows. When combined with IONPs, ultrasound-guided techniques such as MMUS, Focused Ultrasound (FUS) and PA imaging allow the dynamic monitoring of NP distribution, mechanical response, and in vivo therapeutic outcomes. Despite these advantages, most existing reviews that focused on IONPs predominantly emphasize MRI or MPI, while hybrid acoustic and magnetoacoustics techniques remain comparatively underrepresented. Therefore, this review aims to fill this gap in the literature and highlight the growing relevance of methodologies based on the use of ultrasound-guided techniques for diagnosis and therapy combined with IONPs. Figure 1 schematically illustrates the concept of smart IONPs and their potential diagnostic and therapeutic applications in various imaging and treatment modalities.

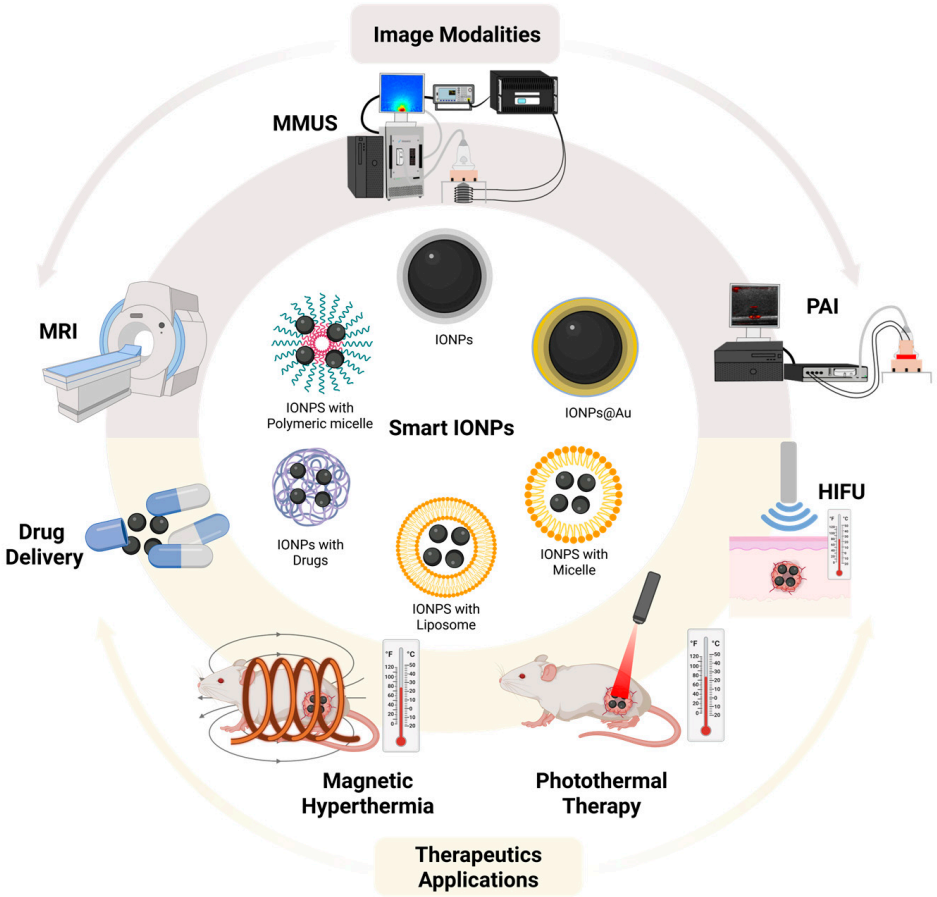

Figure 1. Schematic representation of smart NPs, highlighting their potential use in diagnostic and therapeutic applications.

2. Ultrasound-Guided Diagnosis and Therapy Using NPs

Ultrasound imaging is based on the propagation of high-frequency sound waves through tissues, which are progressively attenuated due to absorption and scattering. The image contrast in most soft tissues arises from the speckle pattern generated by multiple backscattered echoes from variations in acoustic impedance within the tissue. Since

NPs are considerably smaller than the spatial resolution limit of ultrasound, they cannot be directly visualized and are detected indirectly through the effects they induce in the surrounding medium, such as scattering, harmonics, cavitation, or forced movement. In this scenario, MNP-based ultrasonic contrast agents have stood out as multifunctional platforms that combine diagnostic imaging and therapeutic applications, such as MMUS and PAI. In addition to improving image quality, these nanosystems can be designed to respond to ultrasonic stimuli, allowing for the controlled release of drugs directly at the tumor site. This dual functionality maximizes therapeutic efficacy while reducing systemic toxicity [163–165]. One of the main advantages of NPs is their ability to exploit the enhanced permeability and retention (EPR) effect, a characteristic of many solid tumors. Due to the abnormal and highly permeable architecture of tumor vasculature, NPs can extravasate and preferentially accumulate in tumor tissues [166,167]. Furthermore, inefficient lymphatic drainage in the tumor microenvironment further prolongs NP retention, resulting in sustained local drug availability [168,169]. In contrast, normal tissues with endothelial tight junctions restrict NP extravasation, reducing off-target accumulation and adverse side effects [168,170].

2.1. Magnetomotive Ultrasound Imaging (MMUS)

A major challenge in IONP-based therapy is the precise localization of the nanoparticles to guarantee their effective accumulation at the target site [142,143,156]. Another critical aspect is the ability to reliably assess treatment outcomes [143]. A potential solution to both challenges is an emerging technique known as MMUS, which uses magnetic fields to induce motion in IONP, allowing them to be visualized by US [25,107].

MMUS is a technique based on the application of a time-varying external magnetic field that induces motion in tissue where MNPs are accumulated, as well as in their immediate vicinity [24]. When the magnetic field is applied, the NPs experience an attractive force toward the magnet. This force arises from the interaction between the magnetic moment of the particles and the spatial gradient of the applied field and is influenced by intrinsic properties such as magnetic susceptibility and NP volume. The general expression describing this relationship is given by

$$F = \rho V \nabla \left(\vec{M_0} . \vec{B} \right) + \frac{x_{particle}}{\mu_0} \left(\vec{B} . \nabla \right) \vec{B}, \quad (1)$$

where ρ represents the particle density, μ_0 the magnetic permeability, V the volume, $x_{particle}$ the initial susceptibility of the particle (disregarding that of the suspending medium), $\vec{M_0}$ the residual magnetization, and $\vec{B}$ the magnetic flux density [171]. Since biological tissues are weakly diamagnetic, their interaction with the magnetic field is negligible. Superparamagnetic NPs, with susceptibility up to eight orders of magnitude larger, respond strongly to the field and generate the displacement detected in the MMUS [144].

As observed in Equation (1), the measured MMUS signal originates from magnetically induced displacement and is proportional to the effective magnetic volume, magnetic susceptibility, and saturation magnetization of the NPs [144]. Consequently, increasing particle size or the presence of clusters of superparamagnetic NPs intensifies the magnetomotive force, resulting in larger displacements, better signal-to-noise ratio, and potentially improved depth sensitivity or reduced dose requirement [41,136,145,146]. However, IONPs transition from a single-domain superparamagnetic regime to a multi-domain ferro-/ferrimagnetic behavior as size increases, introducing remanent magnetization, which compromises colloidal stability and in vivo safety, thus imposing a practical upper size limit. In addition to size, crystallinity, morphology, and surface coatings critically modulate effective magnetization and force transmission to surrounding tissues: highly crystalline,

multicore, or anisotropic structures exhibit higher saturation magnetization and generate larger dislocations in MMUS than conventional spherical particles under identical excitation. In contrast, surface coatings influence spin disorder at the surface and the magnetization, while decreasing particle–particle interactions and mechanical coupling [41,136,145,146].

Although nanoscale structures cannot be directly visualized with US due to its resolution limits, the displacement generated is on the order of micrometers [172,173] and can be detected at frame rates in the range of kilohertz [174,175]. This sensitivity allows displacements to be mapped, thereby identifying the location of NPs, ensuring their correct positioning, and reducing errors in therapeutic applications such as MH [143,156], in addition to enabling the evaluation of the viscoelastic properties of the local tissue [176].

The implementation of MMUS requires an experimental setup that integrates magnetic field generation with US image acquisition. The system consists of two main modules: a magnetic excitation module, responsible for inducing NPs' motion, and a US imaging unit, responsible for recording and analyzing the resulting displacements. The magnetic excitation module is typically implemented using either an electromagnet driven by a high-power current amplifier or by revolving a permanent magnet [177]. The magnetic excitation can be applied in either an oscillating (sinusoidal) or pulsed form, depending on the application and the desired response. The US unit is synchronized with the magnetic field excitation system via an external trigger, ensuring phase-coherent image acquisition with respect to applied time-varying magnetic field. This synchronization is essential to ensure that the detected displacements correspond to the magnetic excitation, allowing the magnetomotive signal to be distinguished from physiological motion or other sources of noise [178]. In addition, improved localization accuracy and the mitigation of the halo effect—defined as the apparent spatial extension of the magnetomotive response beyond the true MNP distribution—can be achieved by incorporating knowledge on the external magnetic distribution and by employing vectorial detection of the induced displacements [179].

The main advantage of using MNPs as contrast agents is their ability to reach extravascular targets, unlike commercial microbubbles, which remain restricted to the bloodstream [25]. This property, combined with the sensitivity of MMUS, makes the technique particularly promising for molecular imaging, a field of growing interest in medical research and diagnosis [147,175,180]. A schematic representation of the different applications of MMUS is depicted in Figure 2. The molecular imaging functionality of MMUS is related to smart NPs and the different surface coatings that enable the NPs to aggregate in preestablished regions [112,113,131,181,182]. Cells and molecular processes that could not be previously visualized in US due to their size can then be imaged because of the coupled NPs' displacement [175,183,184].

One of the main obstacles to the consolidation of this approach is the efficient generation of magnetic fields capable of inducing measurable displacements without compromising the system integrity or excessively increasing costs. To address this challenge, Valadez et al. [185] developed and evaluated two low-cost magnetic pulse generator circuits: one based on capacitive discharge and the other on a resonant inverter. The results demonstrated that both systems were capable of producing intense magnetic fields, with fast rise times and sufficient stability to induce displacements in biological phantoms on the order of 25 μm, values fully detectable by US. This performance demonstrates that the use of magnetic pulses not only optimizes the MMUS response but also minimizes limitations typical of continuous methods, such as excessive heating and transition noise. A particularly relevant aspect of the study was the observation that the mechanical response of the phantoms varied according to temperature, allowing the estimation of parameters such as shear wave propagation velocity and elastic modulus. These data reveal that the

technique can provide complementary information on tissue properties, while also opening up new possibilities for thermal monitoring [185].

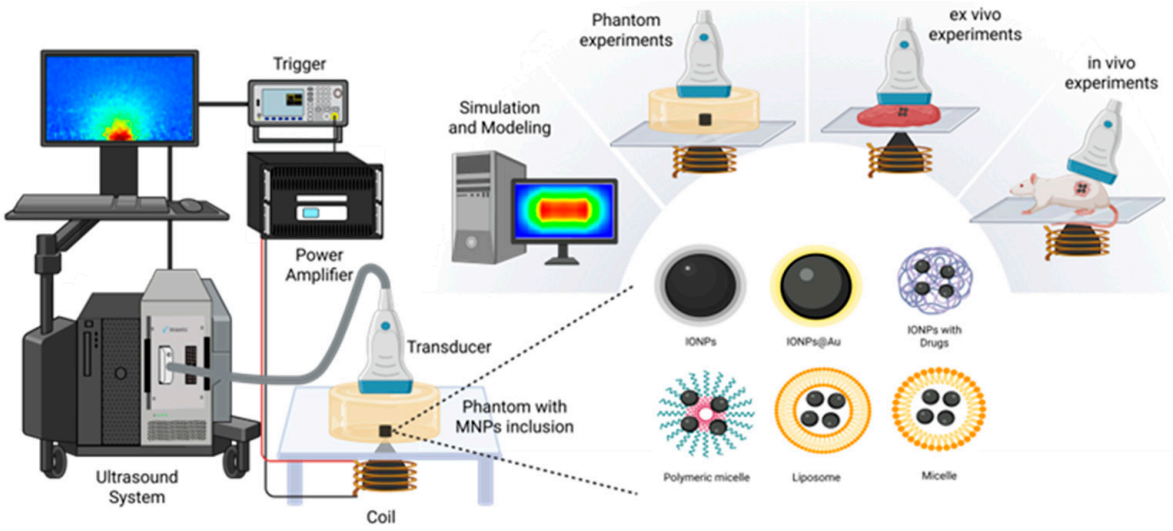

Figure 2. Schematic representation of the different applications of MMUS, from simulations and computational modeling to experiments with phantoms, ex vivo and in vivo.

Shear wave elastography represents another potential application of MMUS [186,187]. In this approach, shear waves are induced by the motion of MNPs, and their velocity is determined by evaluating the temporal delay of displacements at different spatial locations, enabling the reconstruction of the propagating wave [109,187,188]. The shear wave velocity is directly related to the elasticity and viscosity of the medium [187,189], properties that differ in healthy and cancerous tissues [190–192]. Consequently, therapeutic interventions are expected to alter these parameters within the tumor region [193]. By measuring these variations, MMUS-based elastography can be performed, for example, before and after MH to assess treatment efficacy [132,143]. All together, these applications demonstrate the potential of MMUS for solid tumor detection and characterization, integrating molecular and mechanical information within the scope of a single examination.

The functionalization of MNPs enables their accumulation in the tumor microenvironment, beyond the intravascular space, providing targeted molecular contrast that can facilitate the early detection of neoplastic tissues. At the same time, shear wave elastography provides quantitative information on tissue stiffness and viscosity, which are fundamental biomechanical parameters for characterizing neoplastic tissues. Consequently, MMUS emerges as a promising technique for detection, differentiation, and monitoring solid tumors in a sensitive non-invasive manner [151].

Lin et al. (2013) [186], for example, established a finite element-based simulation model to study the influence of various factors on the shear wave velocity in phantoms, and conducted experiments in vivo also. As a result, it was found that the combination of MMUS and shear wave elastography (SWE) allows for the simultaneous detection of MNPs and the evaluation of the local elasticity of the tissue where they are incorporated. The technique showed good sensitivity and resolution, indicating its viability for diagnostic applications, requiring the measurement of the local elasticity with high specificity [186]. In this context, MMUS-SWE is mainly configured as an imaging and mechanical characterization technique, providing spatially resolved information on the presence of magnetic nanoparticles and the local viscoelastic properties of the tissue. The integration of MH with MMUS enables the real-time, quantitative monitoring of thermally induced mechanical alterations in soft tissues, using the same MNPs for both therapeutic heating and imaging-

based quantification. However, these approaches remain focused on the diagnosis and monitoring of tissue response, not constituting, by themselves, a therapeutic control system. Such a theranostic approach would provide a framework for improved control and feedback of MH-based oncological therapies and supports the use of viscoelastic parameters as quantitative clinical biomarkers of tissue response to treatment [176].

Other reports, such as by Sjostrand et al. [194] and Evertsson et al. [138], explored MMUS as a promising imaging alternative for sentinel lymph node (SLN) detection. The SLN is the first regional lymph node to drain the primary tumor and is a key indicator of lymphatic spread [148]. In cases where SLNs are affected by metastases, there is an increase in tissue stiffness, which reduces the displacement amplitude detected by MMUS [148]. This relationship of stiffness and displacement highlights the potential of the technique as a diagnostic tool, capable of replacing intraoperative dyes and radioactive tracers. In addition, its ability to detect MNPs in lymph nodes, the main sites of metastasis, reinforces its use as an auxiliary method in SLN surgery and in the early detection of tumor spread [131]. The results presented by these authors indicate that the use of magnetic microbubbles containing iron oxide nanoparticles (SPION-MBs) significantly increases the magnetomotive signal, overcoming the limitation of low vibration amplitude in rigid tissues. In this context, the sensitivity of the MMUS for detecting NPs is determined by the concentration of NPs and the excitation parameters, namely, the frequency and voltage applied.

A study conducted by researchers at the Swedish Institute for Health Economics, in collaboration with Lund University, evaluated the potential economic value of incorporating an MMUS-based diagnostic system (NanoEcho) for detecting lymph node metastases in patients with rectal cancer, compared to traditional methods. The analysis, conducted from the perspective of the healthcare system, considered only direct costs and used a model consisting of a decision tree followed by a Markov model to simulate clinical evolution over time. In the absence of definitive clinical data on NanoEcho, sensitivity and specificity were assumed to be between 65% and 85%. The model incorporated losses in quality of life associated with radical surgery, permanent stoma, and metastatic disease. The introduction of NanoEcho resulted in an average gain of 0.032 years of life and 0.124 QALYs per patient in the target population. In a cost-neutral scenario, the estimated justifiable prices were 6995 SEK when all patients with rectal cancer were tested and 50,658 SEK when testing was restricted to patients with T1–T2 rectal cancer. When explicitly considering the health gain, assuming a willingness to pay up to 500,000 SEK/QALY, the maximum justifiable price of NanoEcho increases to 10,654 SEK in the first strategy and 65,132 SEK in the second [133]. It is worth noting that, although this study represents only an estimate based on Swedish data and does not necessarily reflect the global scenario for implementing the technique, its results indicate that incorporating the MMUS (NanoEcho) method into the standard protocol of care could potentially reduce healthcare costs and improve the quality of life of patients with rectal cancer [133]. IONPs play a central role in the MMUS approach, generating high-resolution images, improving the accuracy of early diagnosis, and supporting individualized clinical decision-making [133].

In general, recent research in MMUS has focused on consolidating and improving the technique by systematically investigating the parameters that affect its performance, highlighting the need for standardization to enable clinical translation. In this context, although some studies have already explored in vivo applications of MMUS [186,194–196], a substantial portion of the literature still relies on in vitro experiments [132,186], studies in phantoms [41,132,136,182,185,186,197–204], and by numerical simulations [186,198,200,202]. This progression from controlled environments to more complex and realistic scenarios reflects a necessary and well-established methodologi-

cal pathway for validating MMUS, allowing the isolated evaluation of contrast agents, experimental setups, and signal processing algorithms before clinical application.

In summary, we can verify that MMUS can be a powerful ally in cancer diagnosis and treatment, mainly when combined with NPs for tumor targeting and molecular imaging. However, its clinical application is still limited by the low image acquisition speed, which prevents real-time monitoring, and by its need for an external electromagnet, which reduces the portability and practicality of the system [175]. As a recent and emerging technique, MMUS still has large space for improvements. The most recent publications in this area indicate contributions in all parameters related to the performance of the MMUS technique, especially the setup (which includes the coil choice, magnetic field modulation and its integration with therapeutic systems) and the contrast agents combining MNPs to other structures, such as gas vehicles, to enhance MMUS signal.

2.2. Photoacoustic Imaging

PA imaging is a non-invasive technique that combines high optical contrast with the spatial precision of US, enabling real-time imaging in an affordable manner without the use of ionizing radiation [205]. The method is based on the application of laser or LED pulses whose absorption promotes the rapid thermoelastic expansion of tissues, generating transient acoustic waves. These waves are captured by an ultrasonic transducer, enabling the preservation of highly detailed images of biological structures, as illustrated in Figure 3 [206].

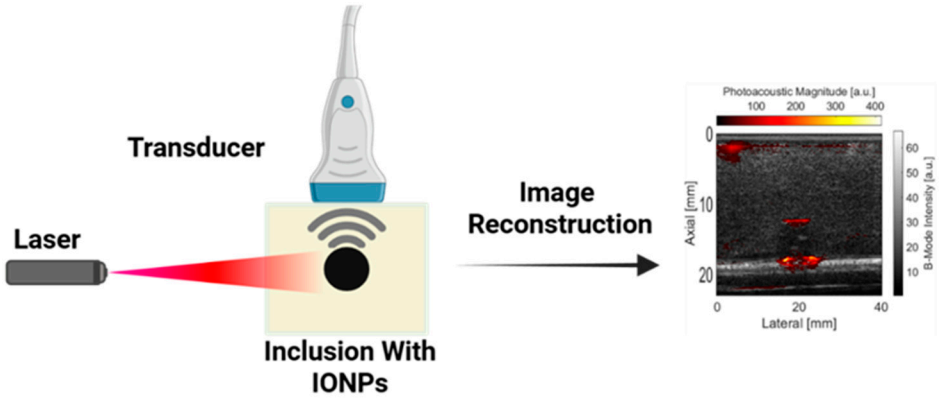

Figure 3. Schematic representation of the operating principle of PA imaging, using a pulsed laser as light-emitting source.

However, the use of NPs with strong optical absorption cross-section allows for the optimization of ultrasonic wave generation, resulting in photoacoustic images with superior contrast and greater applicability in theranostic approaches. However, uncoated IONPs have low observation efficiency in the near-infrared (NIR) region [207,208]. For this purpose, it is essential to incorporate these NPs into matrices such as Natural Rubber Latex (NRL) [146], silica [174], PEG or the deposition of a gold shell [175], NIR-absorbing dyes, or stimuli-responsive polymers, thereby improving optical absorption, the circulation time and tumor-specific accumulation. Such strategies not only increase the contrast and resolution of PA imaging but also allow the same NPs platform to operate as a multifunctional agent for MMUS and MH, establishing a synergistic interplay between diagnostic imaging and therapy.

Alwi et al. [145] investigated the applicability of silica-coated SPIONs as contrast agents for PA imaging in biological environments [138]. Their research was conducted in vitro and ex vivo, using different biological media and tissues to simulate realistic conditions. Among the models tested, sheep serum and blood solutions, as well as avian and

mouse muscle tissue, stood out, allowing the evaluation of both the dispersion and penetration of the PA signal in dense tissues. The silica coating proved effective in maintaining stable dispersion in different media, reducing aggregation, and increasing biocompatibility, without compromising the essential magnetic properties of SPIONs. Cytotoxicity assays indicated low cellular toxicity, confirming their safety for biomedical applications. Measurements demonstrated that silica-coated SPIONs produce significantly more intense PA signals than the background, with a linear response as a function of concentration, confirming their potential for quantification. Experiments on ex vivo tissues reinforced the particles' ability to generate visible contrast at depth, even in highly turbid media [138].

Also, Liu et al. [146] investigated the use of erythrocyte-derived optical NPs (NETs) as contrast agents for PA imaging in live murine models, aiming at the noninvasive detection of coronary artery disease (CAD) and myocardial infarction (MI) [139]. NETs were produced from mouse erythrocyte phantoms, from which hemoglobin had been removed. These structures were doped with the indocyanine green (ICG) dye, giving them optical properties suitable for NIR imaging. PA imaging was performed using a system that combines NIR laser excitation with the detection of acoustic signals generated by light absorption by NETs. This allowed the visualization of atherosclerotic lesions and areas of coronary stenosis in real time, without the need for invasive contrast. The experiments were conducted in live mice, into which NETs were administered intravenously. PA images were acquired at different post-injection times to assess the biodistribution and efficacy of NETs in detecting vascular alterations associated with CAD and MI. ICG-doped NETs allowed a clear visualization of atherosclerotic plaques in mouse coronary arteries, demonstrating their effectiveness as contrast agents for PA imaging. The technique enabled the identification of areas of stenosis in the coronary arteries, correlating with the severity of vascular obstruction. Furthermore, images acquired over time revealed a homogeneous distribution of NETs in the target vascular regions, with a gradual washout of the contrast, indicating favorable pharmacokinetics for clinical applications. Finally, the study demonstrated that ICG-doped NETs are effective and safe contrast agents for PA imaging in live mouse models, allowing the noninvasive detection of atherosclerotic lesions and coronary stenosis [139].

2.3. Hybrid Bioimaging Technique

Hybrid bioimaging techniques combine two or more imaging modalities to overcome the individual limitations of each method while enhancing resolution, sensitivity, and specificity [209]. By integrating complementary contrast mechanisms such as magnetic, acoustic, and optical responses, these approaches enable a more accurate localization, improved visualization of biological structures, and comprehensive assessment of NPs distribution. For example, Evertsson et al. [134] developed an MMUS imaging technique using a novel US approach that incorporates SPIONs as a contrast agent for hybrid imaging, using an SLN rodent as a model to evaluate such an integrated imaging method. One hour after injecting ^{68}Ga-labeled SPIONs, they performed MMUS in combination with PET/CT and MRI. Their findings demonstrated that the nanoplatform effectively enhanced contrast, showing promise for improving the visualization and identification of sentinel lymph nodes in hybrid imaging systems [134].

Furthermore, to increase sensitivity, the MMUS technique was combined with PA images, resulting in the Magnetomotive Photoacoustic Imaging (MPA) modality [208]. In MPA, B-mode and PA images are acquired simultaneously during the application of an external magnetic field. MPA can differentiate healthy from damaged tissues with high depth penetration and image resolution, and can be seen as a synergistic combination of PA imaging and the MMUS technique [210], in which IONPs have been used to improve the efficiency and precision of the technique [208,211]. MPA has already been used to detect

tumor-associated macrophages [212] and to get 3D MPA imaging of tumor xenografts labeled with IONPs in a live animal [140], as illustrated in Figure 4.

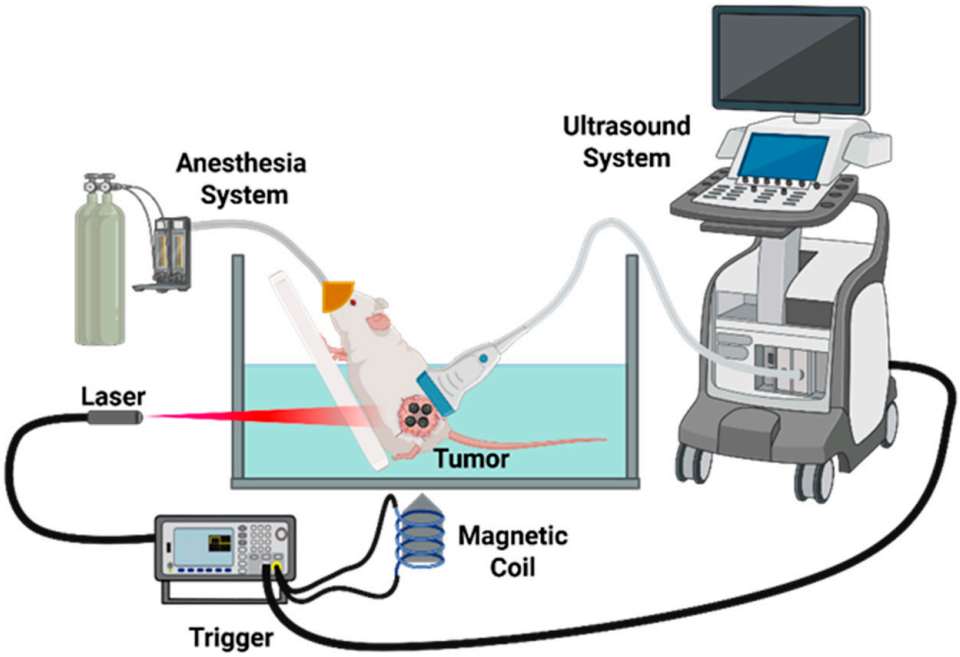

Figure 4. Adapted illustration [140] of the MPA imaging system using an in vivo model.

2.4. FUS-Mediated Hyperthermia and Drug Delivery

Focused Ultrasound (FUS) technology uses high-frequency sound waves to produce thermal or mechanical effects on target tissues. By precisely directing these waves, it can achieve therapeutic results, including non-invasive methods for hyperthermia, drug delivery induced by thermal effects, endothelial disruption, or cavitation. The main advantage of using ultrasonic waves to heat tissues is the possibility of concentrating the beam on a specific region, allowing for the localized deposition of high levels of energy [213–215]. The presence of IONPs enhances the thermal effect of US hyperthermia by increasing the attenuation of ultrasonic waves. This enhancement occurs due to differences in the density, compressibility, and thermal properties of the continuous medium and the dispersed NPs, which, when pulsating and oscillating, generate additional shear and thermal waves. As a result, acoustic energy absorption increases, leading to enhanced local heating [216]. The principle of FUS-mediated hyperthermia in a phantom containing an inclusion of MNPs is schematically presented in Figure 5.

The convergence of diagnostics and therapeutics, known as US-guided nanotheranostics, offers a powerful strategy for precision oncology by enabling the real-time monitoring of drug delivery, treatment response, and tumor regression. Recent developments in this field integrate NPs with dual functions: acting as contrast agents for molecular US imaging while simultaneously serving as carriers for chemotherapeutics, genes, or immunomodulators [158,159]. In fact, mechanical effects (such as acoustic cavitation) and thermal effects, inherent to US, can destabilize NP shells or carrier matrices, triggering a spatiotemporally controlled release of therapeutic payloads. This non-invasive activation not only enhances treatment selectivity but also facilitates deeper tissue penetration, helping to overcome the physical barriers of dense tumor microenvironments [157,160,213,217–219]. For example, Kaczmarek et al. [220] investigated the use of IONPs as enhancers of FUS-induced hyperthermia. For this purpose, the authors used agar gel models simulating biological tissues, some containing specially coated IONPs to ensure dispersion and biocompatibility. These models were

subjected to continuous ultrasonic irradiation at different power levels, and heating was monitored at the focal point and surrounding regions. The results showed that the presence of NPs significantly increases the absorption of ultrasonic energy, leading to higher temperature at the focal point compared to models without NPs. The specific absorption rate (SAR) practically doubled, demonstrating that the NPs act as sonosensitizers, but the temperature did not increase proportionally because the NPs also increase the thermal diffusivity of the gel and the heat dissipation rate to neighboring regions [220].

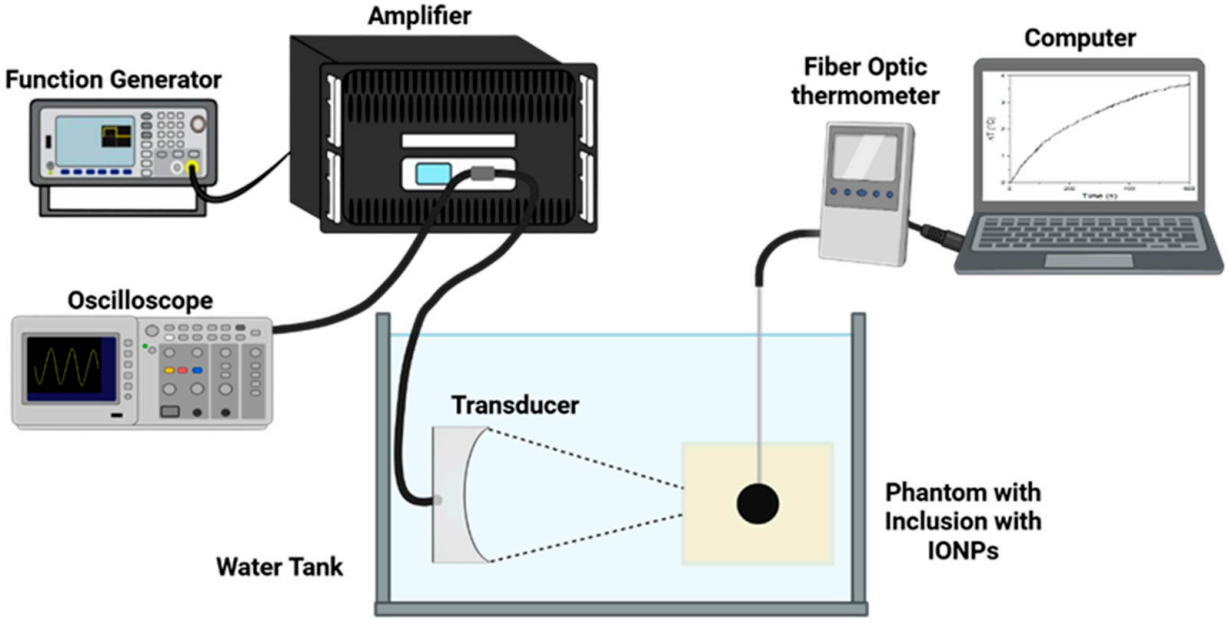

Figure 5. Schematic illustration of the operating principle of FUS-mediated hyperthermia in a phantom containing an inclusion of MNPs.

For drug delivery, Lundy et al. [221] used DOX-loaded liposomes paired with an AP-1 peptide to target IL-4 receptors on glioblastoma (GBM) cells, with FUS increasing drug accumulation in tumors. This approach demonstrated improved chemotherapy delivery with minimal systemic toxicity, increasing drug concentration in tumors by up to 202% in vivo [221]. FUS has also shown to effectively trigger drug release at targeted sites. For example, ANG2-modified PLGA hybrid NPs, co-loaded with DOX and perfluorooctyl bromide, were able to release nearly 50% of their drug cargo within two minutes when exposed to US irradiation at GBM sites. In vivo studies further demonstrated that combining these functionalized NPs with US irradiation significantly extended the median lifespan of GBM-bearing mice to 56 days, compared to 37.5 days for those treated with NPs alone and just 17 days for the control group. Additionally, US techniques offer promising applications in GBM treatment by generating anticancer responses. For example, piezoelectric hybrid lipid–polymeric NPs, functionalized with ApoE and loaded with nutlin-3a, a nongenotoxic drug, were developed. US stimulation was capable of triggering the drug release and activating calcium channels in cancer cells, creating electrical cues with antiproliferative effects. This approach reduced the invasiveness of T98G GBM cells while inducing necrotic and apoptotic cell death, illustrating the potential of US-activated therapies to improve cancer treatment outcomes [161,215,222–225].

2.5. Theranostic Ultrasound

Theranostic US combines diagnosis and therapy in a single platform, enabling not only the precise visualization of tissues and internal structures but also the controlled delivery of treatments. This approach integrates US imaging techniques with therapeutic modalities such as hyperthermia and drug delivery, often using contrast agents or functional NPs to enhance efficacy [226]. By enabling real-time monitoring and targeted interventions, theranostic US represents a promising strategy for less invasive and more personalized treatments, especially for proliferative and cardiovascular disorders. The study conducted by Dennahy et al. [227] developed a nanotheranostic platform designed for cancer diagnosis and treatment, integrating imaging and therapeutic functionalities into a single system. The platform is based on NPs with mesoporous silica capsules functionalized with disulfide-linked hyaluronic acid, providing active tumor targeting and a controlled release of therapeutic agents in reducing environments typical of cancer cells. Within these capsules, perfluorocarbon (PFH) acts as a contrast agent, allowing real-time tumor visualization via US and the monitoring of therapeutic release. For treatment evaluation and application, high-intensity focused ultrasound (HIFU) was used to perform tumor ablation, while conventional US imaging monitored accumulation and assessed tumor response. In vivo testing in mice bearing HeLa-derived tumors demonstrated that the platform selectively accumulated in the tumor, enabled US imaging responsive to the redox environment, and promoted effective synergistic therapy when combined with HIFU [227].

3. IONP-Guided Treatment

3.1. Magneto-Hyperthermia (MH) Treatment

MH relies on the conversion of magnetic energy into thermal energy by MNPs [228,229]. When magnetic NPs are exposed to an alternating magnetic field, they generate heat through magnetic losses, with Néel or Brownian relaxation processes dominating, depending on the particle and surrounding medium properties, as well as the field frequency [149,230,231]. Understanding these mechanisms is crucial for developing efficient NPs for MH [232]. The idea of using heat to treat cancer dates to the 19th century. However, the concept of MH emerged only in the 1950s, with the first studies using heat induction in lymph nodes [233]. In the 1990s, there was significant progress in MH research, with the development of more efficient heating systems and the investigation of the therapeutic potential of IONPs [150,234,235]. This led to the establishment of the MagForce company, which developed an MH system approved in Europe for clinical use in humans in combination with brachytherapy [236,237]. Such a system enables heat delivery to tumor tissue, with temperature monitored by an optical probe, which is also used to monitor NP density in the tumor. The possible applications of smart IONPs in different phases of MH technology development are illustrated in Figure 6.

One of the main advantages of MH is its ability to achieve therapeutic temperatures directly in tumor tissue, minimizing damage to healthy tissues. Additionally, the heat generated by NPs can increase the sensitivity of tumor cells to radiotherapy and chemotherapy, enhancing therapeutic effects [238–242]. However, to get the most out of the technique, it is essential to understand the tumor microenvironment. The tumor microenvironment is a complex ecosystem that influences cancer growth and progression, characterized by hypoxia, acidity, high interstitial pressure, and a dense extracellular matrix. This environment creates favorable conditions for uncontrolled cell proliferation and therapeutic resistance [243]. When administered systemically or directly into the tumor, MNPs can preferentially accumulate in the tumor site due to the enhanced permeability and retention (EPR) effect [244–246]. When exposed to an alternating current (AC) magnetic field—in other words, an oscillating magnetic field—these particles convert magnetic energy into

heat, raising the local temperature and inducing tumor cell death through necrosis or apoptosis [244,245]. In addition to the direct thermal effect, MH can modulate the tumor microenvironment in various ways, enhancing the antitumor immune response [244,247]. The increased temperature can lead to the release of tumor antigens and stress molecules, which can be recognized by immune cells, such as cytotoxic T lymphocytes (CTLs) [244,247]. Moreover, heat can inhibit the function of immunosuppressive cells, such as regulatory T-cells (Tregs), and promote dendritic cell activation, which is essential for antigen presentation to CTLs [244,247]. The combination of MH with other cancer therapies, such as immunotherapy, has been the subject of great interest [247]. Hyperthermia can increase vascular permeability, facilitating the delivery of chemotherapeutic and immunotherapeutic drugs to the tumor [247]. Additionally, it can sensitize tumor cells to radiotherapy, increasing treatment efficacy [247].

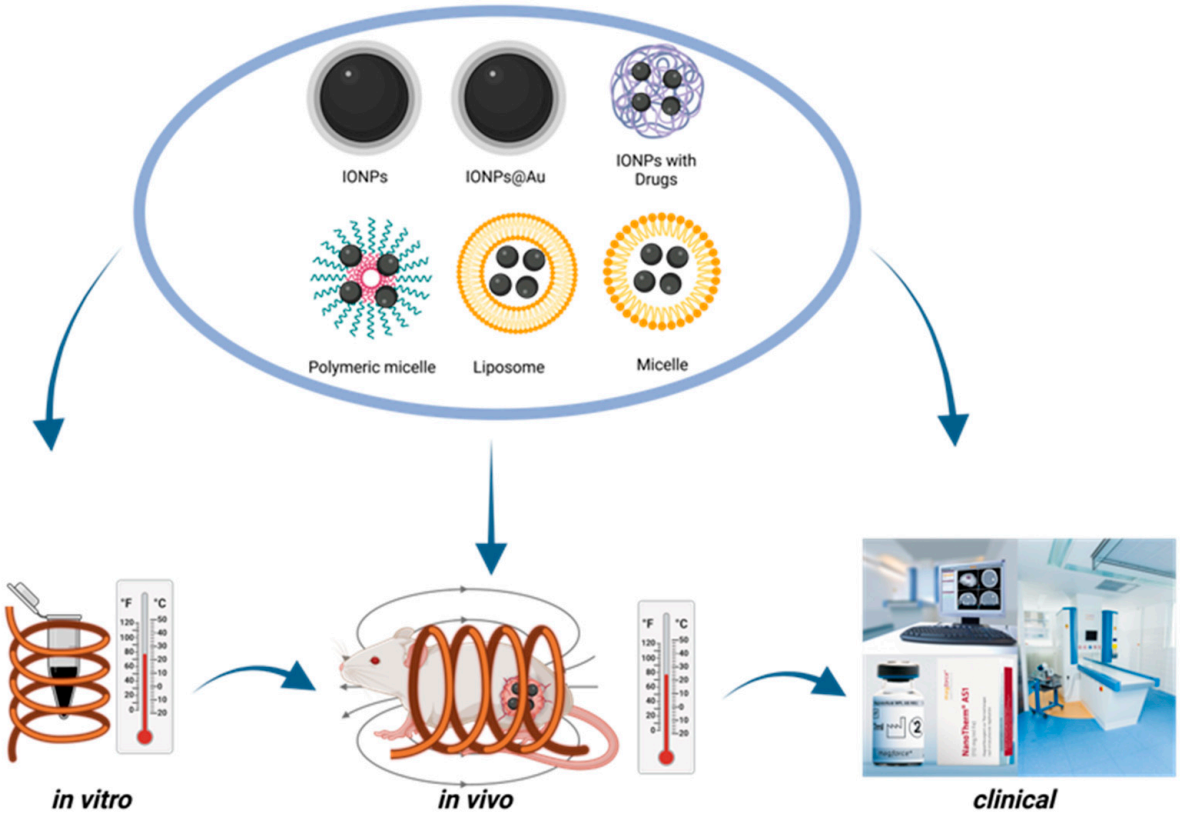

Figure 6. Schematic illustrating the application of NPs in different phases of development of MH technology: in vitro, in vivo and clinical studies.

Despite the therapeutic potential of MH, there are still challenges to be overcome. One of these challenges is to optimize the magnetic field parameters to ensure a uniform and safe heat distribution. One way to control a safe heat distribution is by using the Atkinson–Brezovich limit, which defines the maximum product of field frequency and amplitude that can be applied before significant eddy currents are generated in the system [248].

Non-invasive methods are also required to map the tumor temperature and evaluate the thermal dose delivered. For temperature verification, methods such as photoluminescent thermometry, where multifunctional particles exhibit magnetic properties and emit light in the near-infrared region when heated, allow both temperature detection and the localization of these particles [249,250]. Another approach involves monitoring surface temperature via a thermal camera, which can be combined with the bioheat equation to estimate internal tissue temperatures [151–153]. Additionally, the change in NP density in the medium can be monitored by computed tomography and solving the bioheat equation.

The bioheat equation enables us to determine the thermal dose, called CEM43. This normalization method converts various time–temperature exposures into an equivalent exposure time, expressed in minutes, at the reference temperature of 43 °C [151–153,251,252].

Imaging techniques such as MRI [253] and MPI are also important tools for monitoring and planning MH. These techniques allow visualization of NPs distribution in tumor tissue, assessment of treatment effectiveness, and, in the case of MPI, temperature monitoring [156,254,255]. There are still many challenges regarding MH, but its combination with US techniques can be a promising solution, since US offers the possibility of monitoring NP accumulation by an MMUS [41,136] technique while measuring the temperature with US techniques [143], thus evaluating the precise thermal dose delivered. US techniques are more cost effective than high-end techniques such as MRI and MPI, providing significant economic advantages.

3.2. Magnetic Delivery and Hyperthermia as External Stimuli for Targeted Cancer Therapy

The complexity of cancer has driven researchers to explore therapeutic strategies beyond traditional methods. Whilst active targeting offers advantages over passive targeting, its efficacy remains under 1% when solid tumors are considered [256,257]. To overcome this limitation, integrating external stimulation has emerged as a promising multimodal approach to enhance antitumor effects. Peptide-like target molecules play a crucial role in improving tumor-targeted drug delivery in these strategies. By combining external stimuli with peptide-mediated targeting, researchers aim to increase the precision and effectiveness of drug delivery and treatment of solid tumors. HT external stimulation methods are actively being investigated to improve cancer treatment outcomes [256,257].

Magnetic delivery and hyperthermia are therapeutic strategies that exploit the unique magnetic properties of IONPs such as their superparamagnetic behavior and strong response to external magnetic fields [124,155,162]. In magnetic delivery, external magnetic fields are applied to guide and concentrate NPs at specific target sites, enhancing spatial precision and treatment efficiency. Together, these approaches represent a promising integration of nanotechnology and magnetism for targeted cancer therapy [124,155,162]. Building on this concept, Pucci et al. developed a lipid-based magnetic nanovector (LMNV) functionalized with angiopoietin-2 (ANG2) while encapsulating SPIONs and the chemotherapy agent nutlin-3a. To assess targeting efficiency and blood–brain-barrier (BBB) penetration capability, a microfluidic model using human-derived cells was employed. This dynamic in vitro platform demonstrated that the LMNV successfully accumulated in GBM cells and, upon activation with an alternating magnetic field (AMF), induced apoptosis through the combined effects of MHT and chemotherapy. In vivo studies further confirmed that the ANG2-modified LMNV loaded with temozolomide (TMZ) accumulated effectively in GBM cells without causing toxicity. The synergistic effect of MHT and chemotherapy extended the average survival time to 68 days, compared to 46 days of modified NPs without MHT and 42 days for the control [258].

Similarly, Wang et al. (2016) investigated the use of c(RGDyK) peptide-functionalized and pegylated Fe@Fe_3O_4 NPs (RGD-PEG-MNPs) for MRI and single-photon emission tomography (SPECT)-guided photothermal therapy in U87MG glioblastoma models [259]. The study revealed that, after 6 h of intravenous injection of RGD-PEG-MNPs, the maximum uptake in the tumor was 6.7 ± 1.2% of the injected dose per gram (ID/g), while, in the organs of the mononuclear phagocytic system (MPS), such as liver and spleen, the uptake was significantly lower, with 1.1 ± 0.2% ID/g and 0.16 ± 0.09% ID/g, respectively. These data indicate a significant reduction of uptake by MPS, suggesting an improved biodistribution. Furthermore, MR/SPECT-guided photothermal therapy using RGD-PEG-MNPs demonstrated significant therapeutic efficacy, resulting in a substantial reduction in

tumor volume, indicating improved treatment efficacy. These characteristics make RGD-PEG-MNPs promising as a multifunctional platform for MR/SPECT-guided PTT, with high tumor selectivity and low uptake by MPS, characteristics that may improve biodistribution and therapeutic efficacy in cancer treatments [259].

In another approach, Senturk and colleagues developed curcumin-loaded SPIONs coated with a PLGA-b-PEG diblock copolymer and conjugated with the glycine–arginine–glycine–aspartic acid–serine (GRGDS) peptide, which targets $\alpha v\beta 3/\alpha v\beta 5$ integrins. MHT was applied using a radiofrequency magnetic field, a specific type of AMF. In vitro results showed that GRGDS peptide-conjugated NPs significantly enhanced curcumin bioavailability and reduced the required therapeutic dose by up to six-fold compared to non-conjugated NPs. The combination of GRGDS-functionalized NPs with MHT improved NP uptake through both thermal and non-thermal mechanisms, suggesting a promising approach for the targeted delivery of curcumin to GBM cells. Further studies are needed to fully elucidate the underlying mechanisms of this enhanced uptake [260].

4. Integrating Ultrasound, IONPs and MH

Theranostics is a concept based on the integration of diagnostic and therapeutic functionalities in a single platform, enabling the real-time monitoring of treatment while simultaneously delivering therapeutic agents. IONPs play a central role in this approach, as their magnetic properties allow both therapeutic applications, such as MH, and diagnostic strategies, including MMUS. This dual capability paves the way for precise, image-guided interventions, improving treatment specificity and monitoring in cancer nanomedicine.

Magneto-thermoacoustic imaging is a hybrid technique that generates US contrast from the localized heating of MNPs exposed to alternating or pulsed magnetic fields. The MNPs convert magnetic energy into heat, causing a rapid thermoelastic expansion of the tissue detectable by ultrasonic transducers [261]. This combines the high specific contrast of magnetic probes with the spatial resolution of US. This approach allows mapping the distribution of MNPs in vivo (useful for vector tracking, MH monitoring, and concentration imaging) and can be modulated by static/alternating fields to optimize sensitivity and selectivity [262–264]. Recent studies showed that thermoacoustic mapping can coexist and be harmonized with MMUS techniques, which both opens up opportunities (extraction of multi-mode contrasts) and poses challenges in separating the physical mechanisms and providing quantitative imaging [262,263]. Practical limitations include thermal safety, the heating efficiency of MNPs under biological conditions, and the need for robust algorithms to distinguish thermoelastic contributions from other acoustic effects. Therefore, methodological and contrast agent developments are still ongoing to enable clinical translation [265].

Hadadian et al. [143] integrated MMUS imaging with thermal US strain imaging in conjunction with magnetic induction hyperthermia. Their results indicated that the IONPs served effectively as contrast agents and produced heat during magnetic-induced hyperthermia. Real-time two-dimensional temperature maps were generated, and these findings generally correlated with measurements obtained from a fiber-optic thermometer [143]. Later on, Valadez et al. developed a fully automated system that integrates two complementary techniques in the theranostic field, MMUS and MH [154], as illustrated in Figure 7. The proposal seeks to address one of the main limitations of the clinical application of hyperthermia: precisely locating MNPs in the tissue and monitoring heat distribution in real time during treatment. The authors created a device capable of synchronously switching the magnetic excitation mode to that required by each technique: low-frequency fields, ideal for inducing US-detectable displacements in MMUS, and high-frequency fields, necessary for generating efficient heating in the MH. In this system, the NPs act in dual

mode, allowing the localization (diagnostic) and the treatment: first as contrast agents in MMUS, and second as antennae in MH. This allows mapping the region of interest prior to therapy, ensuring that heat is applied in a targeted manner, reducing risks to healthy tissue. Furthermore, the platform features thermal monitoring, which allows for the real-time control of the heat dose and adjustment of treatment intensity. Experimental results demonstrated that the system can be used to monitor the presence and relative concentration of NPs with MMUS and subsequently correlate this information with the heating profile obtained during MH. This correlation indicates that the displacement detected by US can serve as a predictor of thermal distribution, reinforcing the integration of diagnosis and therapy [154].

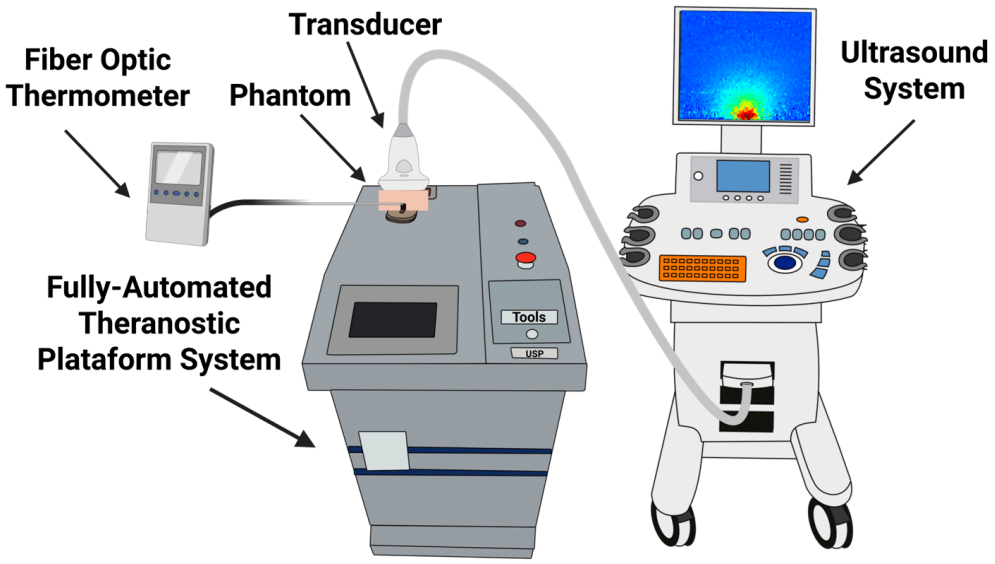

Figure 7. Illustration adapted from the Fully Automated Theranostic Platform System that integrates two complementary techniques: MMUS and MH.

Avoiding incomplete ablation or overtreatment remains a challenge in MH. This issue was addressed by Pi et al. [139], who developed the magnetoacoustic theranostic approach (MATA), a closed-loop theranostic framework that integrates magnetoacoustic ultrasound shear wave elastography (MMUS-SWE) with MH, enabling real-time imaging and treatment feedback [132]. While MMUS-SWE primarily functions as an imaging and mechanical characterization modality, MATA expands this capability by coupling elastographic feedback to therapeutic decision-making during HM [132]. In MATA, ferromagnetic particles (fMPs) serve a dual role: as thermoseeds for MH and shear wave sources for MMUS-SWE. Using magnetic fields, the fMPs generate heat for tumor ablation and produce shear waves to assess changes in tissue stiffness as a measure of treatment success. As a proof of concept, subsequently to an experiment with a phantom, a fresh pork liver sample (8 cm × 4 cm × 3 cm) was used in ex vivo experiments, with a ferromagnetic particle (fMP) implanted at depth of 8 mm. After the MH process and cooling to room temperature, MMUS-SWE was performed to measure the sample's shear wave speed (SWS). Results showed MATA's strong performance in heating and feedback, with significant changes in shear wave speed (from 1.36 to 4.85 m/s) observed in the treated tissue. These results suggest that MATA could offer a novel, integrated approach to tumor treatment and monitoring in clinical settings [132].

Magnetomotive Optical Coherence Tomography (MMOCT) is an imaging technology that utilizes MNPs to generate contrast based on dynamic magnetomotive forces. Unlike MRI and MPI, MMOCT operates with a much lower magnetic field strength, as low as

0.08 Tesla, and can detect ultra-low concentrations of MNP tracers. This technique has been successfully tested in imaging tumor models in animal studies, highlighting its potential for sensitive detection and visualization of pathological tissues. Significant alterations in mechanical resonance frequency were detected exclusively in the group treated with IONPs in MH, suggesting that heat induced increases in the stiffness of melanoma cells. Additionally, changes in tumor stiffness following MH treatment were influenced by factors such as tumor cellularity, protein composition, and temperature elevation. Despite a rise in temperature, tumor softening occurred post-MH due to reduced cellular volume [266].

In vivo applications of magnetomotive optical coherence elastography (MM-OCE) have faced significant limitations, particularly due to long image acquisition times. These delays were primarily caused by the need for extended inter-frame wait periods, implemented to prevent coil overheating from repeated magnetic excitations. The slow imaging process was a major barrier to the practical use of MM-OCE in real-time or dynamic biological systems. Nevertheless, the development of MMOCT has dramatically increased the imaging speed of MM-OCE. In a key experiment, the skin of a mouse was successfully imaged in vivo, achieving a remarkable improvement in image acquisition frequency of at least 414-fold, and post-processing was accelerated 131 times compared to previous methods. Building on these advancements, MM-OCT has also been applied to monitor heat-induced tissue changes. In a separate study, MM-OCT was used to assess stiffness changes in tissue following MH treatment in a melanoma mouse model. The integration of MM-OCT with MNPs enabled the precise tracking of tissue stiffness in real time during and after treatment, demonstrating the theranostic potential (both diagnostic and therapeutic) of this combined approach. These findings suggest that MM-OCT presents potential as a viable dosimetric method, particularly when used with MNPs, holding great promise for monitoring therapeutic outcomes and improving the effectiveness of hyperthermia-based treatments [267].

5. Quantification Challenges in Ultrasound-Guided Nanotheranostics

Despite significant advances in ultrasound-guided theranostic systems based on SPIONs, the accurate quantitative mapping of NPs concentration in vivo remains as a major challenge for most ultrasound-based techniques. In conventional ultrasound and MMUS, signal contrast primarily reflects relative effects such as the displacement of amplitude or mechanical response, which depends not only on NP concentration but also on tissue viscoelasticity, magnetic field distribution, and excitation parameters [24,25,171,175]. Consequently, these methods are predominantly qualitative, enabling the reliable localization of nanoparticle accumulation but not the determination of absolute concentration.

Under controlled conditions, MMUS and PA imaging may provide semi-quantitative information, as signal amplitude can correlate with nanoparticle concentration in phantoms or simplified biological models [107,138,144,268]. However, tissue heterogeneity and physiological variability currently limit robust in vivo quantification. In contrast, MPI offers a true quantitative mapping of IONPs mass, as demonstrated by its linear signal response [93–97]. Accordingly, hybrid approaches combining MPI-based concentration mapping with ultrasound-based techniques, such as MMUS and thermal ultrasound, represent a promising pathway toward quantitative, ultrasound-guided theranostics, especially for improving treatment planning and dose control in MH [143,156,254,255].

6. Translational Challenges and Clinical Readiness

Despite the significant advances in IONP-based ultrasound-guided theranostic systems, several challenges continue to limit their widespread clinical adoption. One of the primary constraints in magnetic hyperthermia and magnetomotive imaging is the need to

operate within safe magnetic field limits, commonly described by the Atkinson limit, which restricts the product of magnetic field amplitude and frequency to avoid excessive eddy current heating and patient discomfort [228,232,246,248,254]. These limitations directly affect heating efficiency, penetration depth, and treatment uniformity in vivo, particularly for deeply seated tumors.

In addition, from an engineering perspective, hardware integration and portability remain critical challenges. Systems that combine ultrasound imaging with magnetic excitation require carefully designed coils, power electronics, and synchronization strategies, which increase system complexity and footprint [24,25,175]. While promising solutions such as compact coil geometries, low-cost pulse generators, and automated excitation–imaging platforms have been reported, further optimization is required to enable portable and clinically practical systems compatible with conventional ultrasound scanners [154,185].

Regulatory considerations also play a central role in clinical translation. Although several IONP formulations have demonstrated biocompatibility and have been approved for clinical use as imaging agents, the endorsement of multifunctional theranostic platforms remains more complex, as it requires the simultaneous validation of safety, efficacy, and manufacturing reproducibility for both diagnostic and therapeutic functions [8,236,237,253,254].

7. Conclusions

The continuous advancement in IONP preparation and surface engineering methods has opened new frontiers in cancer theranostics, enabling the integration of diagnostic and therapeutic functionalities in a single platform. Their magnetic, acoustic, and optical properties in addition to their biocompatibility have proven IONPs to be highly versatile agents for multimodal imaging and targeted therapy. Techniques such as MMUS, PAI, and MH demonstrate that it is possible to combine high-resolution, real-time tumor visualization with minimally invasive treatment, paving the way for personalized and image-guided oncology. Photoacoustic (PA) imaging provides functional and molecular information that cannot be accessed by MMUS alone. While MMUS is uniquely sensitive to the mechanical response induced by magnetically actuated MNPs, enabling nanoparticle localization and tissue stiffness assessment, PA imaging offers contrast based on optical absorption, allowing the evaluation of vascular architecture, hemoglobin concentration, and tissue oxygenation. This capability is particularly relevant for characterizing tumor hypoxia, angiogenesis, and metabolic status, which are critical hallmarks of tumor aggressiveness and therapy resistance. PA imaging is therefore preferred when functional vascular or oxygenation mapping is required, whereas MMUS is better suited for detecting nanoparticle accumulation and mechanical alterations in the tumor microenvironment. When combined, PA and MMUS provide complementary information by simultaneously mapping hypoxia-related functional contrast and nanoparticle-induced mechanical signatures, enabling a more comprehensive characterization of tumor biology and treatment response. Such multimodal integration establishes PA not as a supporting technique, but as a strategic component in ultrasound-guided theranostic systems based on IONPs. MH and US-guided hyperthermia techniques enable precise thermal ablation and enhancement of drug delivery in solid tumors. Moreover, hybrid modalities like magneto-photoacoustic and magneto-thermoacoustic imaging highlight the synergistic potential of integrating magnetic and acoustic phenomena to improve both sensitivity and spatial resolution in preclinical cancer models. Despite these advances, challenges remain regarding the standardization, safety, and translation of these technologies into clinical practice. To overcome these limitations in clinical translation, future efforts should focus on establishing standardized and reproducible protocols for NP synthesis, physicochemical and magnetic characterization, and

dosimetry, ensuring consistency across different platforms and compliance with regulatory requirements. Simultaneously, clinical translation will require the use of biocompatible and scalable manufacturing routes, as well as the development of integrated imaging and therapy systems capable of providing real-time feedback and controlled energy release to ensure treatment safety and efficacy. In summary, the convergence of nanotechnology, US physics, and magnetic nanomaterials represents a promising path toward smarter, more efficient, and patient-specific cancer theranostics. The multimodal integration of MMUS, PAI, and MH guided by US holds the potential to revolutionize how tumors are diagnosed, monitored, and treated, bridging the gap between laboratory innovation and clinical application.

As ultrasound-guided theranostic platforms based on MNPs such as SPIONs continue to evolve toward multimodal and multifunctional systems, the growing complexity of imaging and therapeutic data may benefit from advanced computational tools. In this context, artificial intelligence-based image analysis and multimodal data integration could support the interpretation of complementary ultrasound-derived contrasts, such as magnetomotive displacement, tissue stiffness, and photoacoustic functional signals, without altering the central role of nanoparticles as the active theranostic agents. When appropriately validated, such computational approaches may enhance robustness, reduce operator dependence, and facilitate real-time decision support in complex treatment scenarios, thereby accelerating the clinical translation of nanoparticle-driven ultrasound theranostics.

Author Contributions: Conceptualization, A.A.O.C., T.T.V. and P.P.; methodology, T.T.V., P.P., A.F.S., M.Y.A.N. and N.Z.; formal analysis, T.T.V. and P.P.; investigation (systematic literature search and selection), T.T.V., P.P., A.F.S., M.Y.A.N., N.Z., K.B.S., M.S.B., T.Z.P., K.A. and A.A.O.C.; data curation (organization and critical assessment of published studies), T.T.V., P.P., A.F.S., M.Y.A.N., N.Z., K.B.S., M.S.B., T.Z.P., K.A. and A.A.O.C.; writing—original draft preparation, T.T.V.; writing—review and editing, T.T.V., P.P., A.F.S., M.Y.A.N., N.Z., K.B.S., M.S.B., T.Z.P., K.A. and A.A.O.C.; visualization (figures, schematic illustrations, and graphical synthesis), T.T.V., M.Y.A.N., N.Z. and P.P.; supervision, T.T.V. and A.A.O.C.; project administration, A.A.O.C.; funding acquisition, A.A.O.C. and T.Z.P. All authors have read and agreed to the published version of the manuscript.

Funding: This research was funded by Fundação de Amparo à Pesquisa do Estado de São Paulo (FAPESP) (grants 2018/16939-8, 2021/06728-2, 2023/03371-1, 2022/12771-0, 2023/05357-6 and 2023/11602-3), Conselho Nacional de Desenvolvimento Científico e Tecnológico (CNPq) (grant 311224/2021-0, 311377/2023-8), and Coordenação de Aperfeiçoamento de Pessoal de Nível Superior (CAPES) (finance Code 001).

Institutional Review Board Statement: Not applicable.

Informed Consent Statement: Not applicable.

Data Availability Statement: The original contributions presented in this study are included in the article. Further inquiries can be directed to the corresponding author.

Conflicts of Interest: The authors declare no conflicts of interest.

References

1. Ahmad, M.Y.; Yue, H.; Tegafaw, T.; Liu, S.; Ho, S.L.; Lee, G.H.; Singh, D.; Zhao, X.; Kumar, P.; Chen, Y.; et al. Functionalized lanthanide oxide nanoparticles for tumor targeting, medical imaging, and therapy. *Pharmaceutics* **2021**, *13*, 1890. [CrossRef]
2. Barrios, C.H. Global challenges in breast cancer detection and treatment. *Breast* **2022**, *56*, S3–S6. [CrossRef]
3. de Oliveira Santos, M.; de Lima, F.C.; Martins, L.F.; Oliveira, J.F.; de Almeida, L.M.; de Camargo Cancela, M. Estimativa de Incidência de Câncer no Brasil, 2023–2025. *Rev. Bras. Cancerol.* **2023**, *69*, e-213700. [CrossRef]
4. Bray, F.; Laversanne, M.; Sung, H.; Ferlay, J.; Siegel, R.L.; Soerjomataram, I.; Torre, L.A.; Jemal, A.; Forman, D.; Mathers, C.; et al. Global cancer statistics 2022: GLOBOCAN estimates of incidence and mortality worldwide for 36 cancers in 185 countries. *CA Cancer J. Clin.* **2024**, *74*, 229–263. [CrossRef]

5. Sung, H.; Ferlay, J.; Siegel, R.L.; Laversanne, M.; Soerjomataram, I.; Jemal, A.; Bray, F. Global Cancer Statistics 2020: GLOBOCAN Estimates of Incidence and Mortality Worldwide for 36 Cancers in 185 Countries. *CA Cancer J. Clin.* **2021**, *71*, 209–249. [CrossRef]
6. Schüz, J.; Espina, C. The eleventh hour to enforce rigorous primary cancer prevention. *Mol. Oncol.* **2021**, *15*, 741–743. [CrossRef]
7. Morgan, E.; Arnold, M.; Camargo, M.C.; Gini, A.; Kunzmann, A.T.; Matsuda, T.; Meheus, F.; Verhoeven, R.H.A.; Vignat, J.; Laversanne, M.; et al. The current and future incidence and mortality of gastric cancer in 185 countries, 2020–2040: A population-based modelling study. *eClinicalMedicine* **2022**, *47*, 101404. [CrossRef]
8. Hapuarachchige, S.; Artemov, D. Theranostic Pretargeting Drug Delivery and Imaging Platforms in Cancer Precision Medicine. *Front. Oncol.* **2020**, *10*, 1131. [CrossRef] [PubMed]
9. Cole, J.T.; Holland, N.B. Multifunctional nanoparticles for use in theranostic applications. *Drug Deliv. Transl. Res.* **2015**, *5*, 295–309. [CrossRef] [PubMed]
10. Andre, V.; Abdel-Mottaleb, M.; Shotbolt, M.; Chen, S.; Ramezini, Z.; Zhang, E.; Conlan, S.; Telisman, O.; Liang, P.; Bryant, J.M.; et al. Foundational insights for theranostic applications of magnetoelectric nanoparticles. *Nanoscale Horiz.* **2025**, *10*, 699–718. [CrossRef] [PubMed]
11. Sun, X.; Gong, Y.; Ge, H.; Ma, G.; Yang, T.; Mu, M.; Zhang, L.; Wang, C.; Shen, B.; Dai, X.; et al. Engineered Magnetic Resonance Nanoprobes for Visualizing Tumor Programmed Cell Death Ligand 1 Level and Enhancing Synergistic Radio Immunotherapy. *ACS Nano* **2025**, *19*, 36158–36170. [CrossRef] [PubMed]
12. Trivedi, J.; Yasir, M.; Maurya, R.K.; Tripathi, A.S. Aptamer-based Theranostics in Oncology: Design Strategies and Limitations. *BIO Integr.* **2024**, *5*, 993. [CrossRef]
13. Ayalew, B.D.; Abdullah Mahmood Khan, S.; Getu Alemayehu, Z.; Gifawosen Teferi, M.; Tamrat Aboye, B.; Woldeyohannes, E.M.; Sime, B.L.; Tariku Tewodros, Y.; Inbrahim Hundisa, M. Role of emerging theranostic technologies in precision oncology: Revolutionizing cancer diagnosis and treatment. *Oncologie* **2025**, *27*, 229–238. [CrossRef]
14. Langbein, T.; Weber, W.A.; Eiber, M. Future of theranostics: An outlook on precision oncology in nuclear medicine. *J. Nucl. Med.* **2019**, *60*, 13S–19S. [CrossRef] [PubMed]
15. Filippi, L.; Chiaravalloti, A.; Schillaci, O.; Cianni, R.; Bagni, O. Theranostic approaches in nuclear medicine: Current status and future prospects. *Expert Rev. Med. Devices* **2020**, *17*, 331–343. [CrossRef]
16. Ajinkya, N.; Yu, X.; Kaithal, P.; Luo, H.; Somani, P.; Ramakrishna, S. Magnetic iron oxide nanoparticle (Ionp) synthesis to applications: Present and future. *Materials* **2020**, *13*, 4644. [CrossRef]
17. Attia, N.F.; El-Monaem, E.M.A.; El-Aqapa, H.G.; Elashery, S.E.A.; Eltaweil, A.S.; El Kady, M.; El-Sayed, M.E.; Hassan, H.A.; Mohamed, M.S.; Ahmed, F.A.; et al. Iron oxide nanoparticles and their pharmaceutical applications. *Appl. Surf. Sci. Adv.* **2022**, *11*, 100284. [CrossRef]
18. Dulińska-Litewka, J.; Łazarczyk, A.; Hałubiec, P.; Szafrański, O.; Karnas, K.; Karewicz, A. Superparamagnetic iron oxide nanoparticles-current and prospective medical applications. *Materials* **2019**, *12*, 617. [CrossRef]
19. Petracic, O. Superparamagnetic nanoparticle ensembles. *Superlattices Microstruct.* **2010**, *47*, 569–578. [CrossRef]
20. Schneider, M.G.M.; Martín, M.J.; Otarola, J.; Vakarelska, E.; Simeonov, V.; Lassalle, V.; Nedyalkova, M. Biomedical Applications of Iron Oxide Nanoparticles: Current Insights Progress and Perspectives. *Pharmaceutics* **2022**, *14*, 204. [CrossRef]
21. Meng, Y.Q.; Shi, Y.N.; Zhu, Y.P.; Liu, Y.Q.; Gu, L.W.; Liu, D.D.; Wang, H.; Chen, X.; Li, S.; Zhang, Q.; et al. Recent trends in preparation and biomedical applications of iron oxide nanoparticles. *J. Nanobiotechnol.* **2024**, *22*, 24. [CrossRef] [PubMed]
22. Wang, N.; Zhou, D.; Xu, K.; Kou, D.; Chen, C.; Li, C.; Ge, J.; Chen, L.; Zeng, J.; Gao, M. Iron Homeostasis-Regulated Adaptive Metabolism of PEGylated Ultrasmall Iron Oxide Nanoparticles. *ACS Nano* **2025**, *19*, 13381–13398. [CrossRef]
23. Dadfar, S.M.; Roemhild, K.; Drude, N.I.; von Stillfried, S.; Knüchel, R.; Kiessling, F.; Lammers, T. Iron oxide nanoparticles: Diagnostic, therapeutic and theranostic applications. *Adv. Drug Deliv. Rev.* **2019**, *138*, 302–325. [CrossRef]
24. Oh, J.; Feldman, M.D.; Kim, J.; Condit, C.; Emelianov, S.; Milner, T.E. Detection of magnetic nanoparticles in tissue using magneto-motive ultrasound. *Nanotechnology* **2006**, *17*, 4183–4190. [CrossRef]
25. Sjöstrand, S.; Evertsson, M.; Jansson, T. Magnetomotive Ultrasound Imaging Systems: Basic Principles and First Applications. *Ultrasound Med. Biol.* **2020**, *46*, 2636–2650. [CrossRef]
26. Alam, I.S.; Steinberg, I.; Vermesh, O.; van den Berg, N.S.; Rosenthal, E.L.; van Dam, G.M.; Ntziachristos, V.; Gambir, S.S.; Hernot, S.; Rogalla, S. Emerging Intraoperative Imaging Modalities to Improve Surgical Precision. *Mol. Imaging Biol.* **2018**, *20*, 705–715. [CrossRef]
27. Xie, W.; Guo, Z.; Gao, F.; Gao, Q.; Wang, D.; Liaw, B.S.; Cai, Q.; Sun, X.; Wang, X.; Zhao, L. Shape-, size-and structure-controlled synthesis and biocompatibility of iron oxide nanoparticles for magnetic theranostics. *Theranostics* **2018**, *8*, 3284–3307. [CrossRef]
28. Uchiyama, M.K.; Toma, S.H.; de Rodrigues, S.F.; Shimada, A.L.B.; Loiola, R.A.; Rodríguez, H.J.C.; Oliveira, P.V.; Luz, M.S.; Rabbani, S.R.; Toma, H.E.; et al. Ultrasmall cationic superparamagnetic iron oxide nanoparticles as nontoxic and efficient MRI contrast agent and magnetic-targeting tool. *Int. J. Nanomed.* **2015**, *10*, 4731–4746. [CrossRef]

29. Uchiyama, M.K.; Hebeda, C.B.; Sandri, S.; Paula-Silva, M.; De Romano, M.; Cardoso, R.M.; Toma, S.H.; Araki, K.; Farsky, S.H.P. In vivo evaluation of toxicity and anti-inflammatory activity of iron oxide nanoparticles conjugated with ibuprofen. *Nanomedicine* **2021**, *16*, 741–758. [CrossRef] [PubMed]
30. Romano, M.; Uchiyama, M.K.; Cardoso, R.M.; Toma, S.H.; Baptista, M.S.; Araki, K. Nitric oxide inhibition of lipopolysaccharide-stimulated RAW 247.6 cells by ibuprofen-conjugated iron oxide nanoparticles. *Nanomedicine* **2020**, *15*, 2475–2492. [CrossRef] [PubMed]
31. Lee, N.; Choi, Y.; Lee, Y.; Park, M.; Moon, W.K.; Choi, S.H.; Hyeon, T. Water-dispersible ferrimagnetic iron oxide nanocubes with extremely high r_2 relaxivity for highly sensitive in vivo MRI of tumors. *Nano Lett.* **2012**, *12*, 3127–3131. [CrossRef]
32. Cho, M.; Cervadoro, A.; Ramirez, M.R.; Stigliano, C.; Brazdeikis, A.; Colvin, V.L.; Civera, P.; Key, J.; Decuzzi, P. Assembly of iron oxide nanocubes for enhanced cancer hyperthermia and magnetic resonance imaging. *Nanomaterials* **2017**, *7*, 72. [CrossRef]
33. Sharma, V.K.; Alipour, A.; Soran-Erdem, Z.; Aykut, Z.G.; Demir, H.V. Highly monodisperse low-magnetization magnetite nanocubes as simultaneous T1–T2 MRI contrast agents. *Nanoscale* **2015**, *7*, 10519–10526. [CrossRef]
34. Lee, N.; Kim, H.; Choi, S.H.; Park, M.; Kim, D.; Kim, H.C.; Choi, Y.; Lin, S.; Kim, B.H.; Jung, H.S.; et al. Magnetosome-like ferrimagnetic iron oxide nanocubes for highly sensitive MRI of single cells and transplanted pancreatic islets. *Proc. Natl. Acad. Sci. USA* **2011**, *108*, 2662–2667. [CrossRef] [PubMed]
35. Hu, B.; Zeng, M.; Chen, J.; Zhang, Z.; Zhang, X.; Fan, Z.; Zhang, X. External Magnetic Field-Induced Targeted Delivery of Highly Sensitive Iron Oxide Nanocubes for MRI of Myocardial Infarction. *Small* **2016**, *12*, 4707–4712. [CrossRef] [PubMed]
36. McKiernan, E.P.; Moloney, C.; Chaudhuri, T.R.; Clerkin, S.; Behan, K.; Straubinger, R.M.; Crean, J.; Brougham, D.F. Formation of hydrated PEG layers on magnetic iron oxide nanoflowers shows internal magnetisation dynamics and generates high in-vivo efficacy for MRI and magnetic hyperthermia. *Acta Biomater.* **2022**, *152*, 393–405. [CrossRef] [PubMed]
37. Mohapatra, J.; Mitra, A.; Tyagi, H.; Bahadur, D.; Aslam, M. Iron oxide nanorods as high-performance magnetic resonance imaging contrast agents. *Nanoscale* **2015**, *7*, 9174–9184. [CrossRef]
38. Beg, M.S.; Mohapatra, J.; Pradhan, L.; Patkar, D.; Bahadur, D. Porous Fe_3O_4-SiO_2 core-shell nanorods as high-performance MRI contrast agent and drug delivery vehicle. *J. Magn. Magn. Mater.* **2017**, *428*, 340–347. [CrossRef]
39. Rebolledo, A.F.; Laurent, S.; Calero, M.; Villanueva, A.; Knobel, M.; Marco, J.F.; Tarjat, P. Iron oxide nanosized clusters embedded in porous nanorods: A new colloidal design to enhance capabilities of MRI contrast agents. *ACS Nano* **2010**, *4*, 2095–2103. [CrossRef]
40. Orza, A.; Wu, H.; Xu, Y.; Lu, Q.; Mao, H. One-Step Facile Synthesis of Highly Magnetic and Surface Functionalized Iron Oxide Nanorods for Biomarker-Targeted Applications. *ACS Appl. Mater. Interfaces* **2017**, *9*, 20719–20727. [CrossRef]
41. Arsalani, S.; Hadadian, Y.; Mazon, E.E.; Guidelli, E.J.; Kava, E.; Ramos, A.P.; Gualdi, A.J.; Pavan, T.Z.; Baffa, O.; Carneiro, A.A.O. Uniform size PEGylated iron oxide nanoparticles as a potential theranostic agent synthesized by a simple optimized coprecipitation route. *J. Magn. Magn. Mater.* **2022**, *564*, 170091. [CrossRef]
42. Karimzadeh, I.; Aghazadeh, M.; Doroudi, T.; Ganjali, M.R.; Kolivand, P.H. Superparamagnetic iron oxide (Fe_3O_4) nanoparticles coated with PEG/PEI for biomedical applications: A facile and scalable preparation route based on the cathodic electrochemical deposition method. *Adv. Phys. Chem.* **2017**, *2017*, 9437487. [CrossRef]
43. Arami, H.; Stephen, Z.; Veiseh, O.; Zhang, M. Chitosan-coated iron oxide nanoparticles for molecular imaging and drug delivery. In *Chitosan for Biomaterials I*; Springer: Berlin/Heidelberg, Germany, 2011. [CrossRef]
44. Yilmaz, H.; Sanlier, S.H. Preparation of magnetic gelatin nanoparticles and investigating the possible use as chemotherapeutic agent. *Artif. Cells Nanomed. Biotechnol.* **2013**, *41*, 69–77. [CrossRef] [PubMed]
45. Nosrati, H.; Sefidi, N.; Sharafi, A.; Danafar, H.; Kheiri Manjili, H. Bovine Serum Albumin (BSA) coated iron oxide magnetic nanoparticles as biocompatible carriers for curcumin-anticancer drug. *Bioorg. Chem.* **2018**, *76*, 501–509. [CrossRef]
46. Quan, Q.; Xie, J.; Gao, H.; Yang, M.; Zhang, F.; Liu, G.; Lin, X.; Wang, A.; Eden, H.S.; Lee, S.; et al. HSA coated iron oxide nanoparticles as drug delivery vehicles for cancer therapy. *Mol. Pharm.* **2011**, *8*, 1669–1676. [CrossRef]
47. Sodipo, B.K.; Aziz, A.A.; Mustapa, M. Facile synthesis and characteristics of gold coated superparamagnetic iron oxide nanoparticles via sonication. *Int. J. Nanoelectron. Mater.* **2015**, *8*, 1–6.
48. Foglia, S.; Ledda, M.; Fioretti, D.; Iucci, G.; Papi, M.; Capellini, G.; Lolli, M.G.; Grimaldi, S.; Rinaldi, M.; Lisi, A. In vitro biocompatibility study of sub-5 nm silica-coated magnetic iron oxide fluorescent nanoparticles for potential biomedical application. *Sci. Rep.* **2017**, *7*, srep46513. [CrossRef]
49. Arsalani, S.; Guidelli, E.J.; Silveira, M.A.; Salmon, C.E.G.; Araujo, J.F.D.F.; Bruno, A.C.; Baffa, O. Magnetic Fe_3O_4 nanoparticles coated by natural rubber latex as MRI contrast agent. *J. Magn. Magn. Mater.* **2019**, *475*, 458–464. [CrossRef]
50. Ahmadpoor, F.; Masood, A.; Feliu, N.; Parak, W.J.; Shojaosadati, S.A. The Effect of Surface Coating of Iron Oxide Nanoparticles on Magnetic Resonance Imaging Relaxivity. *Front. Nanotechnol.* **2021**, *3*, 644734. [CrossRef]
51. Stein, R.; Friedrich, B.; Mühlberger, M.; Cebulla, N.; Schreiber, E.; Tietze, R.; Cicha, I.; Alexiou, C.; Dutz, S.; Boccaccini, A.R.; et al. Synthesis and characterization of citrate-stabilized gold-coated superparamagnetic iron oxide nanoparticles for biomedical applications. *Molecules* **2020**, *25*, 4425. [CrossRef]

52. Kim, E.H.; Ahn, Y.; Lee, H.S. Biomedical applications of superparamagnetic iron oxide nanoparticles encapsulated within chitosan. *J. Alloys Compd.* **2007**, *434–435*, 633–636. [CrossRef]
53. Gupta, A.K.; Gupta, M. Synthesis and surface engineering of iron oxide nanoparticles for biomedical applications. *Biomaterials* **2005**, *26*, 3995–4021. [CrossRef]
54. Sun, S.N.; Wei, C.; Zhu, Z.Z.; Hou, Y.L.; Venkatraman, S.S.; Xu, Z.C. Magnetic iron oxide nanoparticles: Synthesis and surface coating techniques for biomedical applications. *Chin. Phys. B* **2014**, *23*, 037503. [CrossRef]
55. Stueber, D.D.; Villanova, J.; Aponte, I.; Xiao, Z.; Colvin, V.L. Magnetic nanoparticles in biology and medicine: Past, present, and future trends. *Pharmaceutics* **2021**, *13*, 943. [CrossRef]
56. Anik, M.I.; Hossain, M.K.; Hossain, I.; Mahfuz, A.M.U.B.; Rahman, M.T.; Ahmed, I. Recent progress of magnetic nanoparticles in biomedical applications: A review. *Nano Sel.* **2021**, *2*, 1146–1186. [CrossRef]
57. Soetaert, F.; Korangath, P.; Serantes, D.; Fiering, S.; Ivkov, R. Cancer therapy with iron oxide nanoparticles: Agents of thermal and immune therapies. *Adv. Drug Deliv. Rev.* **2020**, *163–164*, 65–83. [CrossRef] [PubMed]
58. Abd Elrahman, A.A.; Mansour, F.R. Targeted magnetic iron oxide nanoparticles: Preparation, functionalization and biomedical application. *J. Drug Deliv. Sci. Technol.* **2019**, *52*, 702–712. [CrossRef]
59. Tong, L.; Zhao, M.; Zhu, S.; Chen, J. Synthesis and application of superparamagnetic iron oxide nanoparticles in targeted therapy and imaging of cancer. *Front. Med. China* **2011**, *5*, 379–387. [CrossRef] [PubMed]
60. Krishnan, K.M. Biomedical nanomagnetics: A spin through possibilities in imaging, diagnostics, and therapy. *IEEE Trans. Magn.* **2010**, *46*, 2523–2558. [CrossRef]
61. Li, Z.; Wang, C.; Cheng, L.; Gong, H.; Yin, S.; Gong, Q.; Li, Y.; Liu, Z. PEG-functionalized iron oxide nanoclusters loaded with chlorin e6 for targeted, NIR light induced, photodynamic therapy. *Biomaterials* **2013**, *34*, 9160–9170. [CrossRef] [PubMed]
62. Wang, Y.; Wei, G.; Zhang, X.; Huang, X.; Zhao, J.; Guo, X.; Zhou, S. Multistage Targeting Strategy Using Magnetic Composite Nanoparticles for Synergism of Photothermal Therapy and Chemotherapy. *Small* **2018**, *14*, e1702994. [CrossRef] [PubMed]
63. Tiwari, G.; Tiwari, R.; Bannerjee, S.; Bhati, L.; Pandey, S.; Pandey, P.; Bannerjee, S.K. Drug delivery systems: An updated review. *Int. J. Pharm. Investig.* **2012**, *2*, 2–11. [CrossRef]
64. Feng, Q.; Zhang, Y.; Zhang, W.; Hao, Y.; Wang, Y.; Zhang, H.; Hou, L.; Zhang, Z. Programmed near-infrared light-responsive drug delivery system for combined magnetic tumor-targeting magnetic resonance imaging and chemo-phototherapy. *Acta Biomater.* **2017**, *49*, 402–413. [CrossRef] [PubMed]
65. Ma, X.; Tao, H.; Yang, K.; Feng, L.; Cheng, L.; Shi, X.; Li, Y.; Guo, L.; Liu, Z. A functionalized graphene oxide-iron oxide nanocomposite for magnetically targeted drug delivery, photothermal therapy, and magnetic resonance imaging. *Nano Res.* **2012**, *5*, 199–212. [CrossRef]
66. Fu, X.; Wang, X.; Zhou, S.; Zhang, Y. IONP-doped nanoparticles for highly effective NIR-controlled drug release and combination tumor therapy. *Int. J. Nanomed.* **2017**, *12*, 3751–3766. [CrossRef]
67. Manjusha, V.; Rajeev, M.R.; Anirudhan, T.S. Magnetic nanoparticle embedded chitosan-based polymeric network for the hydrophobic drug delivery of paclitaxel. *Int. J. Biol. Macromol.* **2023**, *235*, 123900. [CrossRef]
68. Guo, L.; Chen, H.; He, N.; Deng, Y. Effects of surface modifications on the physicochemical properties of iron oxide nanoparticles and their performance as anticancer drug carriers. *Chin. Chem. Lett.* **2018**, *29*, 1829–1833. [CrossRef]
69. Can, H.K.; Kavlak, S.; ParviziKhosroshahi, S.; Güner, A. Preparation, characterization and dynamical mechanical properties of dextran-coated iron oxide nanoparticles (DIONPs). *Artif. Cells Nanomed. Biotechnol.* **2018**, *46*, 421–431. [CrossRef]
70. Tran, T.T.D.; Van Vo, T.; Tran, P.H.L. Design of iron oxide nanoparticles decorated oleic acid and bovine serum albumin for drug delivery. *Chem. Eng. Res. Des.* **2015**, *94*, 112–118. [CrossRef]
71. Ferreira, M.; Sousa, J.; Pais, A.; Vitorino, C. The role of magnetic nanoparticles in cancer nanotheranostics. *Materials* **2020**, *13*, 266. [CrossRef]
72. Hola, K.; Markova, Z.; Zoppellaro, G.; Tucek, J.; Zboril, R. Tailored functionalization of iron oxide nanoparticles for MRI, drug delivery, magnetic separation and immobilization of biosubstances. *Biotechnol. Adv.* **2015**, *33*, 1162–1176. [CrossRef]
73. Liang, P.C.; Chen, Y.C.; Chiang, C.F.; Mo, L.R.; Wei, S.Y.; Hsieh, W.Y.; Lin, W.L. Doxorubicin-modified magnetic nanoparticles as a drug delivery system for magnetic resonance imaging-monitoring magnet-enhancing tumor chemotherapy. *Int. J. Nanomed.* **2016**, *11*, 2021–2037. [CrossRef]
74. Mosafer, J.; Teymouri, M.; Abnous, K.; Tafaghodi, M.; Ramezani, M. Study and evaluation of nucleolin-targeted delivery of magnetic PLGA-PEG nanospheres loaded with doxorubicin to C6 glioma cells compared with low nucleolin-expressing L929 cells. *Mater. Sci. Eng. C* **2017**, *72*, 123–133. [CrossRef]
75. Ji, F.; Zhang, K.; Li, J.; Gu, Y.; Zhao, J.; Zhang, J. A Dual pH/Magnetic Responsive Nanocarrier Based on PEGylated Fe_3O_4 Nanoparticles for Doxorubicin Delivery. *J. Nanosci. Nanotechnol.* **2017**, *18*, 4464–4470. [CrossRef] [PubMed]
76. Zaloga, J.; Pöttler, M.; Leitinger, G.; Friedrich, R.P.; Almer, G.; Lyer, S.; Baum, E.; Tietze, R.; Heimke-Brinck, R.; Mangge, H.; et al. Pharmaceutical formulation of HSA hybrid coated iron oxide nanoparticles for magnetic drug targeting. *Eur. J. Pharm. Biopharm.* **2016**, *101*, 152–162. [CrossRef] [PubMed]

77. Romaní-Cubells, E.; Martinez-Erro, S.; Morales, V.; van Grieken, R.; García Muñoz, R.A.; Sanz, R. Mitoxantrone-Derivative Drug Structure-Directing Agent for the Synthesis of Magnetic Mesoporous Silica Nanoparticles for Breast Cancer Treatment. *ACS Appl. Nano Mater.* **2024**, *7*, 12376–12386. [CrossRef]
78. Li, Y.; Zhou, H.; Zhao, Z.; Yan, S.; Chai, Y. Mitoxantrone encapsulated photosensitizer nanomicelle as carrier-free theranostic nanomedicine for near-infrared fluorescence imaging-guided chemo-photodynamic combination therapy on cancer. *Int. J. Pharm.* **2024**, *655*, 124025. [CrossRef] [PubMed]
79. Singh, A.; Bora, S.; Khurana, S.; Kumar, P.; Sarkar, N.; Kukreti, R.; Kaushik, M. Advance nanotherapeutic approach for systemic co-delivery of mitoxantrone loaded chitosan coated PLGA nanoparticles to improve the chemotherapy against human non-small cell lung cancer. *J. Drug Deliv. Sci. Technol.* **2023**, *84*, 104523. [CrossRef]
80. Mansouri, M.; Nazarpak, M.H.; Solouk, A.; Akbari, S.; Hasani-Sadrabadi, M.M. Magnetic responsive of paclitaxel delivery system based on SPION and palmitoyl chitosan. *J. Magn. Magn. Mater.* **2017**, *421*, 316–325. [CrossRef]
81. Shobhana, N.; Naveen, N.R.; Goudanavar, P. Magnetic precision: Unleashing the therapeutic potential of paclitaxel-loaded nanoparticles in breast cancer treatment. *Oral Oncol. Rep.* **2024**, *10*, 100283. [CrossRef]
82. Masoumi Godgaz, S.; Asefnejad, A.; Bahrami, S.H. Fabrication of PEGylated SPIONs-Loaded Niosome for Codelivery of Paclitaxel and Trastuzumab for Breast Cancer Treatment: In Vivo Study. *ACS Appl. Bio Mater.* **2024**, *7*, 2951–2965. [CrossRef] [PubMed]
83. Chen, H.A.; Lu, Y.J.; Dash, B.S.; Chao, Y.K.; Chen, J.P. Hyaluronic Acid-Modified Cisplatin-Encapsulated Poly(Lactic-co-Glycolic Acid) Magnetic Nanoparticles for Dual-Targeted NIR-Responsive Chemo-Photothermal Combination Cancer Therapy. *Pharmaceutics* **2023**, *15*, 290. [CrossRef]
84. Sahoo, B.; Devi, K.S.P.; Dutta, S.; Maiti, T.K.; Pramanik, P.; Dhara, D. Biocompatible mesoporous silica-coated superparamagnetic manganese ferrite nanoparticles for targeted drug delivery and MR imaging applications. *J. Colloid Interface Sci.* **2014**, *431*, 31–41. [CrossRef]
85. Frullano, L.; Meade, T.J. Multimodal MRI contrast agents. *J. Biol. Inorg. Chem.* **2007**, *12*, 939–949. [CrossRef]
86. Unterweger, H.; Janko, C.; Schwarz, M.; Dézsi, L.; Urbanics, R.; Matuszak, J.; Őrfi, E.; Fülöp, T.; Bäuerle, T.; Szebeni, J.; et al. Non-immunogenic dextran-coated superparamagnetic iron oxide nanoparticles: A biocompatible, size-tunable contrast agent for magnetic resonance imaging. *Int. J. Nanomed.* **2017**, *12*, 5223–5238. [CrossRef] [PubMed]
87. Chertok, B.; Moffat, B.A.; David, A.E.; Yu, F.; Bergemann, C.; Ross, B.D.; Yang, V.C. Iron oxide nanoparticles as a drug delivery vehicle for MRI monitored magnetic targeting of brain tumors. *Biomaterials* **2008**, *29*, 487–496. [CrossRef]
88. Israel, L.L.; Galstyan, A.; Holler, E.; Ljubimova, J.Y. Magnetic iron oxide nanoparticles for imaging, targeting and treatment of primary and metastatic tumors of the brain. *J. Control. Release* **2020**, *320*, 45–62. [CrossRef]
89. Lazaro-Carrillo, A.; Filice, M.; Guillén, M.J.; Amaro, R.; Viñambres, M.; Tabero, A.; Ovejero Paredes, K.; Villanueva, A.; Calvo, P.; Morales, M.P.; et al. Tailor-made PEG coated iron oxide nanoparticles as contrast agents for long lasting magnetic resonance molecular imaging of solid cancers. *Mater. Sci. Eng. C* **2020**, *107*, 110262. [CrossRef]
90. Luo, S.; Ma, C.; Zhu, M.Q.; Ju, W.N.; Yang, Y.; Wang, X. Application of Iron Oxide Nanoparticles in the Diagnosis and Treatment of Neurodegenerative Diseases With Emphasis on Alzheimer's Disease. *Front. Cell. Neurosci.* **2020**, *14*, 21. [CrossRef] [PubMed]
91. Qiao, R.; Fu, C.; Forgham, H.; Javed, I.; Huang, X.; Zhu, J.; Whittaker, A.K.; Davis, T.P. Magnetic iron oxide nanoparticles for brain imaging and drug delivery. *Adv. Drug Deliv. Rev.* **2023**, *197*, 114822. [CrossRef] [PubMed]
92. Ramanathan, S.; Archunan, G.; Sivakumar, M.; Selvan, S.T.; Fred, A.L.; Kumar, S.; Gulyás, B.; Padmanabhan, P. Theranostic applications of nanoparticles in neurodegenerative disorders. *Int. J. Nanomed.* **2018**, *13*, 5561–5576. [CrossRef]
93. Billings, C.; Langley, M.; Warrington, G.; Mashali, F.; Johnson, J.A. Magnetic particle imaging: Current and future applications, magnetic nanoparticle synthesis methods and safety measures. *Int. J. Mol. Sci.* **2021**, *22*, 7651. [CrossRef]
94. Gleich, B.; Borgert, J.; Weizenecker, J. Magnetic Particle Imaging (MPI). *Medicamundi* **2006**, *50*, 66–71. [CrossRef]
95. Du, Y.; Liu, X.; Liang, Q.; Liang, X.J.; Tian, J. Optimization and Design of Magnetic Ferrite Nanoparticles with Uniform Tumor Distribution for Highly Sensitive MRI/MPI Performance and Improved Magnetic Hyperthermia Therapy. *Nano Lett.* **2019**, *19*, 3618–3626. [CrossRef] [PubMed]
96. Dadfar, S.M.; Camozzi, D.; Darguzyte, M.; Roemhild, K.; Varvarà, P.; Metselaar, J.; Banala, S.; Straub, M.; Güvener, N.; Engelmann, U.; et al. Size-isolation of superparamagnetic iron oxide nanoparticles improves MRI, MPI and hyperthermia performance. *J. Nanobiotechnol.* **2020**, *18*, 22. [CrossRef] [PubMed]
97. Bauer, L.M.; Situ, S.F.; Griswold, M.A.; Samia, A.C.S. High-performance iron oxide nanoparticles for magnetic particle imaging-guided hyperthermia (hMPI). *Nanoscale* **2016**, *8*, 12162–12169. [CrossRef]
98. Weller, D.; Salamon, J.M.; Frölich, A.; Möddel, M.; Knopp, T.; Werner, R. Combining Direct 3D Volume Rendering and Magnetic Particle Imaging to Advance Radiation-Free Real-Time 3D Guidance of Vascular Interventions. *Cardiovasc. Interv. Radiol.* **2020**, *43*, 322–330. [CrossRef]
99. Zhou, X.Y.; Tay, Z.W.; Chandrasekharan, P.; Yu, E.Y.; Hensley, D.W.; Orendorff, R.; Jeffris, K.E.; Mai, D.; Zheng, B.; Goodwill, P.W.; et al. Magnetic particle imaging for radiation-free, sensitive and high-contrast vascular imaging and cell tracking. *Curr. Opin. Chem. Biol.* **2018**, *45*, 131–138. [CrossRef]

100. Weizenecker, J.; Gleich, B.; Rahmer, J.; Dahnke, H.; Borgert, J. Three-dimensional real-time in vivo magnetic particle imaging. *Phys. Med. Biol.* **2009**, *54*, L1. [CrossRef] [PubMed]
101. Ludewig, P.; Graeser, M.; Forkert, N.D.; Thieben, F.; Rández-Garbayo, J.; Rieckhoff, J.; Lessmann, K.; Förger, F.; Szwargulski, P.; Magnus, T.; et al. Magnetic particle imaging for assessment of cerebral perfusion and ischemia. *Wiley Interdiscip. Rev. Nanomed. Nanobiotechnol.* **2022**, *14*, e1757. [CrossRef]
102. Meola, A.; Rao, J.; Chaudhary, N.; Song, G.; Zheng, X.; Chang, S.D. Magnetic Particle Imaging in Neurosurgery. *World Neurosurg.* **2019**, *125*, 261–270. [CrossRef] [PubMed]
103. Wu, X.L.C.; Zhang, X.Y.; Steinberg, X.G.; Qu, X.H.; Huang, X.S.; Cheng, X.M.; Bliss, T.; Du, F.; Rao, J.; Song, G.; et al. A review of magnetic particle imaging and perspectives on neuroimaging. *Am. J. Neuroradiol.* **2019**, *40*, 206–212. [CrossRef] [PubMed]
104. Du, Y.; Lai, P.T.; Leung, C.H.; Pong, P.W.T. Design of superparamagnetic nanoparticles for magnetic particle imaging (MPI). *Int. J. Mol. Sci.* **2013**, *14*, 18682–18710. [CrossRef] [PubMed]
105. Bulte, J.W.; Walczak, P.; Janowski, M.; Krishnan, K.M.; Arami, H.; Halkola, A.; Gleich, B.; Rahmer, J. Quantitative "Hot-Spot" Imaging of Transplanted Stem Cells Using Superparamagnetic Tracers and Magnetic Particle Imaging. *Tomography* **2015**, *1*, 91–97. [CrossRef]
106. Zheng, B.; Von See, M.P.; Yu, E.; Gunel, B.; Lu, K.; Vazin, T.; Schaffer, D.V.; Goodwill, P.W.; Conolly, S.M. Quantitative magnetic particle imaging monitors the transplantation, biodistribution, and clearance of stem cells in vivo. *Theranostics* **2016**, *6*, 291–301. [CrossRef]
107. Mehrmohammadi, M.; Qu, M.; Ma, L.L.; Romanovicz, D.K.; Johnston, K.P.; Sokolov, K.V.; Emelianov, S.Y. Pulsed magneto-motive ultrasound imaging to detect intracellular accumulation of magnetic nanoparticles. *Nanotechnology* **2011**, *22*, 415105. [CrossRef]
108. Huber, C.M.; Pavan, T.Z.; Ullmann, I.; Heim, C.; Rupitsch, S.J.; Vossiek, M.; Alexiou, C.; Ermert, H.; Lyer, S. A Review on Ultrasound-based Methods to Image the Distribution of Magnetic Nanoparticles in Biomedical Applications. *Ultrasound Med. Biol.* **2025**, *51*, 210–234. [CrossRef]
109. Sampaio, D.R.T.; Grillo, F.W.; Bruno, A.C.; Pavan, T.Z.; Carneiro, A.A.O. A magneto-motive ultrasound platform designed for pre-clinical and clinical applications. *Rev. Bras. Eng. Biomed.* **2016**, *32*, 337–346. [CrossRef]
110. Evertsson, M.; Cinthio, M.; Kjellman, P.; Fredriksson, S.; Andersson, R.; Toftevall, H.; Persson, W.H.; Jansson, T. In vivo magnetomotive ultrasound imaging of rat lymph nodes—A pilot study. In Proceedings of the 2015 IEEE International Ultrasonics Symposium (IUS), Taipei, Taiwan, 21–24 October 2015. [CrossRef]
111. Qu, M.; Mehrmohammadi, M.; Emelianov, S. Detection of nanoparticle endocytosis using magneto-photoacoustic imaging. *Small* **2011**, *7*, 2858–2862. [CrossRef]
112. Thomas, R.; Park, I.K.; Jeong, Y.Y. Magnetic iron oxide nanoparticles for multimodal imaging and therapy of cancer. *Int. J. Mol. Sci.* **2013**, *14*, 15910–15930. [CrossRef]
113. Kanazaki, K.; Sano, K.; Makino, A.; Shimizu, Y.; Yamauchi, F.; Ogawa, S.; Ding, N.; Yano, T.; Temma, T.; Ono, M.; et al. Development of anti-HER2 fragment antibody conjugated to iron oxide nanoparticles for in vivo HER2-targeted photoacoustic tumor imaging. *Nanomed. Nanotechnol. Biol. Med.* **2015**, *11*, 2051–2060. [CrossRef]
114. Fernandes, G.S.P.; Uliana, J.H.; Bachmann, L.; Carneiro, A.A.O.; Lediju Bell, M.A.; Pavan, T.Z. Mitigating skin tone bias in linear array in vivo photoacoustic imaging with short-lag spatial coherence beamforming. *Photoacoustics* **2023**, *33*, 100555. [CrossRef]
115. Xu, M.; Wang, L.V. Photoacoustic imaging in biomedicine. *Rev. Sci. Instrum.* **2006**, *77*, 041101. [CrossRef]
116. Peng, J.R.; Qi, T.T.; Liao, J.F.; Chu, B.Y.; Yang, Q.; Qu, Y.; Li, W.; Li, H.; Luo, F.; Qian, Z. Mesoporous magnetic gold "nanoclusters" as theranostic carrier for chemo-photothermal co-therapy of breast cancer. *Theranostics* **2014**, *4*, 678. [CrossRef]
117. Johannsen, M.; Thiesen, B.; Wust, P.; Jordan, A. Magnetic nanoparticle hyperthermia for prostate cancer. *Int. J. Hyperth.* **2010**, *26*, 790–795. [CrossRef]
118. Robles, J.; Das, R.; Glassell, M.; Phan, M.H.; Srikanth, H. Exchange-coupled $Fe_3O_4/CoFe_2O_4$ nanoparticles for advanced magnetic hyperthermia. *AIP Adv.* **2018**, *8*, 056719. [CrossRef]
119. Gavilán, H.; Avugadda, S.K.; Fernández-Cabada, T.; Soni, N.; Cassani, M.; Mai, B.T.; Chantrell, R.; Pellegrino, T. Magnetic nanoparticles and clusters for magnetic hyperthermia: Optimizing their heat performance and developing combinatorial therapies to tackle cancer. *Chem. Soc. Rev.* **2021**, *50*, 11614–11667. [CrossRef] [PubMed]
120. Nemati, Z.; Alonso, J.; Rodrigo, I.; Das, R.; Garaio, E.; García, J.Á.; Orue, I.; Phan, M.-H.; Srikanth, H.l. Improving the Heating Efficiency of Iron Oxide Nanoparticles by Tuning Their Shape and Size. *J. Phys. Chem. C* **2018**, *122*, 2367–2381. [CrossRef]
121. Ortega, D.; Pankhurst, Q.A. Magnetic hyperthermia. *Nanoscience* **2012**, *1*, e88. [CrossRef]
122. Brero, F.; Calzolari, P.; Albino, M.; Antoccia, A.; Arosio, P.; Berardinelli, F.; Bettega, D.; Ciocca, M.; Facoetti, A.; Gallo, S.; et al. Proton Therapy, Magnetic Nanoparticles and Hyperthermia as Combined Treatment for Pancreatic BxPC3 Tumor Cells. *Nanomaterials* **2023**, *13*, 791. [CrossRef]
123. Wang, Y.; Zou, L.; Qiang, Z.; Jiang, J.; Zhu, Z.; Ren, J. Enhancing Targeted Cancer Treatment by Combining Hyperthermia and Radiotherapy Using Mn-Zn Ferrite Magnetic Nanoparticles. *ACS Biomater. Sci. Eng.* **2020**, *6*, 3550–3562. [CrossRef]

124. Guisasola, E.; Asín, L.; Beola, L.; De La Fuente, J.M.; Baeza, A.; Vallet-Regí, M. Beyond Traditional Hyperthermia: In Vivo Cancer Treatment with Magnetic-Responsive Mesoporous Silica Nanocarriers. *ACS Appl. Mater. Interfaces* **2018**, *10*, 12518–12525. [CrossRef]
125. Tian, Z.; Yu, X.; Ruan, Z.; Zhu, M.; Zhu, Y.; Hanagata, N. Magnetic mesoporous silica nanoparticles coated with thermo-responsive copolymer for potential chemo- and magnetic hyperthermia therapy. *Microporous Mesoporous Mater.* **2018**, *256*, 1–9. [CrossRef]
126. Estelrich, J.; Antònia Busquets, M. Iron oxide nanoparticles in photothermal therapy. *Molecules* **2018**, *23*, 1567. [CrossRef]
127. Ji, X.; Shao, R.; Elliott, A.M.; Jason Stafford, R.; Esparza-Coss, E.; Bankson, J.A.; Liang, G.; Luo, Z.-P.; Park, K.; Markert, J.T.; et al. Bifunctional Gold Nanoshells with a Superparamagnetic Iron Oxide-Silica Core Suitable for Both MR Imaging and Photothermal Therapy. *J. Phys. Chem. C* **2007**, *111*, 6245–6251. [CrossRef]
128. Hou, X.; Wang, X.; Liu, R.; Zhang, H.; Liu, X.; Zhang, Y. Facile synthesis of multifunctional Fe_3O_4@SiO_2@Au magneto-plasmonic nanoparticles for MR/CT dual imaging and photothermal therapy. *RSC Adv.* **2017**, *7*, 18844–18850. [CrossRef]
129. Hu, R.; Zheng, M.; Wu, J.; Li, C.; Shen, D.; Yang, D.; Li, L.; Ge, M.; Chang, Z.; Dong, W. Core-shell magnetic gold nanoparticles for magnetic field-enhanced radio-photothermal therapy in cervical cancer. *Nanomaterials* **2017**, *7*, 111. [CrossRef] [PubMed]
130. Dongsar, T.T.; Dongsar, T.S.; Abourehab, M.A.S.; Gupta, N.; Kesharwani, P. Emerging application of magnetic nanoparticles for breast cancer therapy. *Eur. Polym. J.* **2023**, *187*, 111898. [CrossRef]
131. Evertsson, M.; Kjellman, P.; Cinthio, M.; Fredriksson, S.; in 't Zandt, R.; Persson, H.; Jansson, T. Multimodal detection of iron oxide nanoparticles in rat lymph nodes using magnetomotive ultrasound imaging and magnetic resonance imaging. *IEEE Trans. Ultrason. Ferroelectr. Freq. Control* **2014**, *61*, 1276–1283. [CrossRef] [PubMed]
132. Pi, Z.; Deng, D.; Chen, X.; Chen, S.; Lin, H.; Chen, M. Magneto-Acoustic Theranostic Approach: Integration of Magnetomotive Ultrasound Shear Wave Elastography and Magnetic Hyperthermia. *J. Ultrasound Med.* **2024**, *43*, 1819–1831. [CrossRef]
133. Andersson, E.; Axelsson, U.; Rönnow, C.F.; Thorlacius, H.; Persson, L.; Fridhammar, A. The Potential Health Economic Value of Adding Magnetomotive Ultrasound to Current Diagnostic Methods for Detecting Lymph Node Metastases in Rectal Cancer. *Pharmacoeconomics* **2025**, *43*, 779–791. [CrossRef]
134. Evertsson, M.; Kjellman, P.; Cinthio, M.; Andersson, R.; Tran, T.A.; in 't Zandt, R.; Grafström, G.; Toftevall, H.; Fredriksson, S.; Ingvar, C.; et al. Combined Magnetomotive ultrasound, PET/CT, and MR imaging of 68Ga-labelled superparamagnetic iron oxide nanoparticles in rat sentinel lymph nodes in vivo. *Sci. Rep.* **2017**, *7*, 4824. [CrossRef]
135. Periyathambi, P.; Vicente, T.T.; Uliana, J.H.; da Silva Prado, M.E.C.; Gualdi, A.J.; Pavan, T.Z.; Carneiro, A.A.O. Oleic acid-coated iron oxide nanoparticles for enhanced magnetomotive ultrasound and photoacoustic imaging in oil-based phantoms. *Mater. Lett.* **2026**, *403*, 139409. [CrossRef]
136. Arsalani, S.; Arsalani, S.; Isikawa, M.; Guidelli, E.J.; Mazon, E.E.; Ramos, A.P.; Bakuzis, A.; Pavan, T.Z.; Baffa, O.; Carneiro, A.A.O. Hybrid Nanoparticles of Citrate-Coated Manganese Ferrite and Gold Nanorods in Magneto-Optical Imaging and Thermal Therapy. *Nanomaterials* **2023**, *13*, 434. [CrossRef]
137. Vale, A.C.A.R.; Monte, R.S.; Das, A.; de Azevedo, L.A.; Silva, R.B.; Gomes, A.S.L.; Júnior, S.A. Synthesis and characterization of hybrid mesoporous silica-iron oxide nanocomposite as a potential contrast agent for photoacoustic imaging. *Next Mater.* **2025**, *9*, 100992. [CrossRef]
138. Alwi, R.; Telenkov, S.; Mandelis, A.; Leshuk, T.; Gu, F.; Oladepo, S.; Michaelian, K. Silica-coated super paramagnetic iron oxide nanoparticles (SPION) as biocompatible contrast agent in biomedical photoacoustics. *Biomed. Opt. Express* **2012**, *3*, 2500–2509. [CrossRef] [PubMed]
139. Liu, Y.; Hanley, T.; Chen, H.; Long, S.R.; Gambhir, S.S.; Cheng, Z.; Wu, J.C.; El Fakhri, G.; Anvari, B.; Zaman, R.T.; et al. Non-Invasive Photoacoustic Imaging of In Vivo Mice with Erythrocyte Derived Optical Nanoparticles to Detect CAD/MI. *Sci. Rep.* **2020**, *10*, 5983. [CrossRef]
140. Qu, M.; Mehrmohammadi, M.; Truby, R.; Graf, I.; Homan, K.; Emelianov, S. Contrast-enhanced magneto-photo-acoustic imaging in vivo using dual-contrast nanoparticles. *Photoacoustics* **2014**, *2*, 55–62. [CrossRef] [PubMed]
141. Mehrmohammadi, M.; Oh, J.; Mallidi, S.; Emelianov, S.Y. Pulsed magneto-motive ultrasound imaging using ultrasmall magnetic nanoprobes. *Mol. Imaging* **2011**, *10*, 102–110. [CrossRef] [PubMed]
142. Fink, M.; Rupitsch, S.J.; Lyer, S.; Ermert, H. Quantitative Determination of Local Density of Iron Oxide Nanoparticles Used for Drug Targeting Employing Inverse Magnetomotive Ultrasound. *IEEE Trans. Ultrason. Ferroelectr. Freq. Control* **2021**, *68*, 2482–2495. [CrossRef]
143. Hadadian, Y.; Uliana, J.H.; Carneiro, A.A.O.; Pavan, T.Z. A Novel Theranostic Platform: Integration of Magnetomotive and Thermal Ultrasound Imaging with Magnetic Hyperthermia. *IEEE Trans. Biomed. Eng.* **2021**, *68*, 68–77. [CrossRef] [PubMed]
144. Mehrmohammadi, M.; Shin, T.H.; Qu, M.; Kruizinga, P.; Truby, R.L.; Lee, J.-H.; Cheon, J.; Emelianov, S.Y. In vivo pulsed magneto-motive ultrasound imaging using high-performance magnetoactive contrast nanoagents. *Nanoscale* **2013**, *5*, 11179–11186. [CrossRef]

145. Arsalani, S.; Arsalani, S.; Hadadian, Y.; Sampaio, D.R.T.; Baffa, O.; Pavan, T.Z.; Carneiro, A.A.O. The effect of magnetization of natural rubber latex-coated magnetite nanoparticles on shear wave dispersion magneto-motive ultrasound. *Phys. Med. Biol.* **2019**, *64*, 215019. [CrossRef] [PubMed]
146. Vicente, T.T.; Arsalani, S.; Quiel, M.S.; Fernandes, G.S.; da Silva, K.R.; Fukada, S.Y.; Gualdi, A.J.; Guidelli, É.J.; Baffa, O.; Carneiro, A.A.; et al. Improving the Theranostic Potential of Magnetic Nanoparticles by Coating with Natural Rubber Latex for Ultrasound, Photoacoustic Imaging, and Magnetic Hyperthermia: An In Vitro Study. *Pharmaceutics* **2024**, *16*, 1474. [CrossRef]
147. Hadadian, Y.; Ramos, A.P.; Sampaio, D.; Carneiro, A.; Pavan, T. Magneto-motive ultrasound imaging using superparamagnetic ferrite nanoparticles with enhanced saturation magnetization synthesized by a simple copreciptation method. In Proceedings of the 2017 IEEE International Ultrasonics Symposium (IUS), Washington, DC, USA, 6–9 September 2017. [CrossRef]
148. Madru, R.; Kjellman, P.; Olsson, F.; Wingårdh, K.; Ingvar, C.; Ståhlberg, F.; Olsrud, J.; Lätt, J.; Fredriksson, S.; Knutsson, L.; et al. 99mTc-labeled superparamagnetic iron oxide nanoparticles for multimodality SPECT/MRI of sentinel lymph nodes. *J. Nucl. Med.* **2012**, *53*, 459–463. [CrossRef]
149. Torres, T.E.; Lima, E.; Calatayud, M.P.; Sanz, B.; Ibarra, A.; Fernández-Pacheco, R.; Mayoral, Á.; Marquina, C.; Ibarra, M.R.; Goya, G.F. The relevance of Brownian relaxation as power absorption mechanism in Magnetic Hyperthermia. *Sci. Rep.* **2019**, *9*, 3992. [CrossRef] [PubMed]
150. Jordan, A.; Scholz, R.; Wust, P.; Fähling, H.; Krause, J.; Wlodarczyk, W.; Sander, B.; Vogl, T.; Felix, R. Effects of Magnetic Fluid Hyperthermia (MFH) on C3H mammary carcinoma in vivo. *Int. J. Hyperth.* **1997**, *13*, 587–605. [CrossRef]
151. Capistrano, G.; Rodrigues, H.F.; Zufelato, N.; Gonçalves, C.; Cardoso, C.G.; Silveira-Lacerda, E.P.; Bakuzis, A.F. Noninvasive intratumoral thermal dose determination during in vivo magnetic nanoparticle hyperthermia: Combining surface temperature measurements and computer simulations. *Int. J. Hyperth.* **2020**, *37*, 120–140. [CrossRef]
152. Rodrigues, H.F.; Capistrano, G.; Mello, F.M.; Zufelato, N.; Silveira-Lacerda, E.; Bakuzis, A.F. Precise determination of the heat delivery during in vivo magnetic nanoparticle hyperthermia with infrared thermography. *Phys. Med. Biol.* **2017**, *62*, 4062. [CrossRef]
153. Rodrigues, H.F.; Mello, F.M.; Branquinho, L.C.; Zufelato, N.; Silveira-Lacerda, E.P.; Bakuzis, A.F. Real-time infrared thermography detection of magnetic nanoparticle hyperthermia in a murine model under a non-uniform field configuration. *Int. J. Hyperth.* **2013**, *29*, 752–767. [CrossRef]
154. Valadez, E.E.M.; Uliana, J.H.; Vicente, T.T.; Carneiro, A.A.O.; Pavan, T.Z. Fully-Automated Theranostic System Integrating Magnetomotive Ultrasound and Magnetic Hyperthermia. *IEEE Trans. Instrum. Meas.* **2025**, *74*, 4002911. [CrossRef]
155. Patri, S.; Thanh, N.T.K.; Kamaly, N. Magnetic iron oxide nanogels for combined hyperthermia and drug delivery for cancer treatment. *Nanoscale* **2024**, *16*, 15446–15464. [CrossRef]
156. Tay, Z.W.; Chandrasekharan, P.; Chiu-Lam, A.; Hensley, D.W.; Dhavalikar, R.; Zhou, X.Y.; Yu, E.Y.; Goodwill, P.W.; Zheng, B.; Rinaldi, C.; et al. Magnetic Particle Imaging-Guided Heating in Vivo Using Gradient Fields for Arbitrary Localization of Magnetic Hyperthermia Therapy. *ACS Nano* **2018**, *12*, 3699–3713. [CrossRef] [PubMed]
157. Patrick, P.S.; Stuckey, D.J.; Zhu, H.; Kalber, T.L.; Iftikhar, H.; Southern, P.; Bear, J.C.; Lythgoe, M.F.; Hattersley, S.R.; Pankhurst, Q.A. Improved tumour delivery of iron oxide nanoparticles for magnetic hyperthermia therapy of melanoma via ultrasound guidance and 111In SPECT quantification. *Nanoscale* **2024**, *16*, 19715–19729. [CrossRef] [PubMed]
158. Li, C.H.; Chang, Y.C.; Hsiao, M.; Chan, M.H. Ultrasound and Nanomedicine for Cancer-Targeted Drug Delivery: Screening, Cellular Mechanisms and Therapeutic Opportunities. *Pharmaceutics* **2022**, *14*, 1282. [CrossRef]
159. Entzian, K.; Aigner, A. Drug delivery by ultrasound-responsive nanocarriers for cancer treatment. *Pharmaceutics* **2021**, *13*, 1135. [CrossRef]
160. Moradi Kashkooli, F.; Jakhmola, A.; Hornsby, T.K.; Tavakkoli, J.; Kolios, M.C. Ultrasound-mediated nano drug delivery for treating cancer: Fundamental physics to future directions. *J. Control. Release* **2023**, *355*, 552–578. [CrossRef]
161. Yang, F.Y.; Wong, T.T.; Teng, M.C.; Liu, R.S.; Lu, M.; Liang, H.F.; Wei, M.-C. Focused ultrasound and interleukin-4 receptor-targeted liposomal doxorubicin for enhanced targeted drug delivery and antitumor effect in glioblastoma multiforme. *J. Control. Release* **2012**, *160*, 652–658. [CrossRef] [PubMed]
162. Sumitha, N.S.; Krishna, N.G.; Sailaja, G.S. Multifunctional chitosan ferrogels for targeted cancer therapy by on-demand magnetically triggered drug delivery and hyperthermia. *Biomater. Adv.* **2022**, *142*, 213137. [CrossRef]
163. Su, Y.; Huang, L.; Zhang, D.; Zeng, Z.; Hong, S.; Lin, X. Recent Advancements in Ultrasound Contrast Agents Based on Nanomaterials for Imaging. *ACS Biomater. Sci. Eng.* **2024**, *10*, 5496–5512. [CrossRef]
164. Yang, X.; Zhao, M.; Wu, Z.; Chen, C.; Zhang, Y.; Wang, L.; Guo, Q.; Wang, Q.; Liang, S.; Hu, S.; et al. Nano-ultrasonic Contrast Agent for Chemoimmunotherapy of Breast Cancer by Immune Metabolism Reprogramming and Tumor Autophagy. *ACS Nano* **2022**, *16*, 3417–3431. [CrossRef]
165. Fang, J.; Tan, J.; Lin, L.; Cao, Y.; Xu, R.; Lin, C.; He, G.; Xu, X.; Xiao, X.; Jiang, Q.; et al. Bioactive Nanotherapeutic Ultrasound Contrast Agent for Concurrent Breast Cancer Ultrasound Imaging and Treatment. *Adv. Healthc. Mater.* **2024**, *13*, 2401436. [CrossRef]

166. Yang, H.; Cai, W.; Xu, L.; Lv, X.; Qiao, Y.; Li, P.; Wu, H.; Yang, Y.; Zhang, L.; Duan, Y. Nanobubble-Affibody: Novel ultrasound contrast agents for targeted molecular ultrasound imaging of tumor. *Biomaterials* **2015**, *37*, 279–288. [CrossRef] [PubMed]
167. Nel, A.; Ruoslahti, E.; Meng, H. New Insights into "permeability" as in the Enhanced Permeability and Retention Effect of Cancer Nanotherapeutics. *ACS Nano* **2017**, *11*, 9567–9569. [CrossRef] [PubMed]
168. Ejigah, V.; Owoseni, O.; Bataille-Backer, P.; Ogundipe, O.D.; Fisusi, F.A.; Adesina, S.K. Approaches to Improve Macromolecule and Nanoparticle Accumulation in the Tumor Microenvironment by the Enhanced Permeability and Retention Effect. *Polymers* **2022**, *14*, 2601. [CrossRef] [PubMed]
169. Kalyane, D.; Raval, N.; Maheshwari, R.; Tambe, V.; Kalia, K.; Tekade, R.K. Employment of enhanced permeability and retention effect (EPR): Nanoparticle-based precision tools for targeting of therapeutic and diagnostic agent in cancer. *Mater. Sci. Eng. C* **2019**, *98*, 1252–1276. [CrossRef]
170. Huang, D.; Sun, L.; Huang, L.; Chen, Y. Nanodrug delivery systems modulate tumor vessels to increase the enhanced permeability and retention effect. *J. Pers. Med.* **2021**, *11*, 124. [CrossRef]
171. Shevkoplyas, S.S.; Siegel, A.C.; Westervelt, R.M.; Prentiss, M.G.; Whitesides, G.M. The force acting on a superparamagnetic bead due to an applied magnetic field. *Lab Chip* **2007**, *7*, 1294–1302. [CrossRef]
172. Hossain, M.M.; Levy, B.E.; Thapa, D.; Oldenburg, A.L.; Gallippi, C.M. Blind Source Separation-Based Motion Detector for Imaging Super-Paramagnetic Iron Oxide (SPIO) Particles in Magnetomotive Ultrasound Imaging. *IEEE Trans. Med. Imaging* **2018**, *37*, 2356–2366. [CrossRef]
173. Levy, B.E.; Hossain, M.M.; Sierchio, J.M.; Thapa, D.; Gallippi, C.M.; Oldenburg, A.L. Effect of model thrombus volume and elastic modulus on magnetomotive ultrasound signal under pulsatile flow. *IEEE Trans. Ultrason. Ferroelectr. Freq. Control* **2018**, *65*, 1380–1388. [CrossRef]
174. Mazon, E.E.; Arsalani, S.; Uliana, J.H.; Carneiro, A.A.O.; Gualdi, A.J.; Pavan, T.Z. A pulsed magnetomotive ultrasound imaging system for magnetic nanoparticle detection. In Proceedings of the 2021 IEEE UFFC Latin America Ultrasonics Symposium (LAUS), Gainesville, FL, USA, 4–5 October 2021. [CrossRef]
175. Shen, W.H.; Li, M.L. Toward Real Time Backward-Mode Pulsed Magnetomotive Ultrasound. In Proceedings of the 2019 IEEE International Ultrasonics Symposium (IUS), Glasgow, UK, 6–9 October 2019.
176. Freire, J.E.; Collazos-Burbano, D.A.; Uliana, J.H.; Zufelato, N.; Carneiro, A.A.; Carson, P.L.; Pavan, T.Z. Pulsed magnetomotive ultrasound for viscoelastic characterization of soft tissues during magnetic hyperthermia. *Phys. Med. Biol.* **2025**, *70*, 225003. [CrossRef]
177. Strachen, N.; Booske, J.; Behdad, N. A mechanically based magneto-inductive transmitter with electrically modulated reluctance. *PLoS ONE* **2018**, *13*, e0199934. [CrossRef]
178. Evertsson, M.; Cinthio, M.; Fredriksson, S.; Olsson, F.; Persson, H.; Jansson, T. Frequency-and phase-sensitive magnetomotive ultrasound imaging of superparamagnetic iron oxide nanoparticles. *IEEE Trans. Ultrason. Ferroelectr. Freq. Control* **2013**, *60*, 481–491. [CrossRef]
179. Collazos-Burbano, D.A.; Freire, J.E.; Sanches, A.F.; Zufelato, N.; Uliana, J.H.; Brassesco, M.S.; Carneiro, A.A.O.; Pavan, T.Z. Beyond Axial Symmetry: Tracking Vectorial Motion Enhances Nanoparticles Mapping With Magnetomotive Ultrasound. *IEEE Access* **2025**, *13*, 62704–62716. [CrossRef]
180. Rowe, S.P.; Pomper, M.G. Molecular imaging in oncology: Current impact and future directions. *CA Cancer J. Clin.* **2022**, *72*, 333–352. [CrossRef]
181. Li, F.; Lu, J.; Kong, X.; Hyeon, T.; Ling, D. Dynamic Nanoparticle Assemblies for Biomedical Applications. *Adv. Mater.* **2017**, *29*, 1605897. [CrossRef] [PubMed]
182. Kim, W.S.; Min, S.; Kim, S.K.; Kang, S.; An, S.; Criado-Hidalgo, E.; Davis, H.; Bar-Zion, A.; Malounda, D.; Kim, Y.H.; et al. Magneto-acoustic protein nanostructures for non-invasive imaging of tissue mechanics in vivo. *Nat. Mater.* **2024**, *23*, 290–300. [CrossRef]
183. Fink, M.; Ermert, H.; Lyer, S.; Alexiou, C. Influence of naturally occurring tissue movements on magnetomotive ultrasound detection of iron oxide nanoparticles for magnetic drug targeting. In Proceedings of the 2017 IEEE International Ultrasonics Symposium (IUS), Washington, DC, USA, 6–9 September 2017. [CrossRef]
184. Lu, M.C.; Houng, J.Y.; Li, M.L. Backward-mode ultrafast pulsed magnetomotive ultrasound. In Proceedings of the 2017 IEEE International Ultrasonics Symposium (IUS), Washington, DC, USA, 6–9 September 2017. [CrossRef]
185. Mazon Valadez, E.E.; Bordonal, R.R.; Freire, J.E.; Uliana, J.H.; Arsalani, S.; Collazos-Burbano, D.A.; Carneiro, A.A.; Pavan, T.Z. Pulse generators for enhanced magnetomotive ultrasound: Toward a cost-effective imaging for tissue characterization. *Rev. Sci. Instrum.* **2024**, *95*, 074904. [CrossRef] [PubMed]
186. Lin, H.; Chen, T.; Deng, D.; Pi, Z.; Xie, S.; Ding, G. Magnetomotive Ultrasound Shear Wave Elastography (MMUS-SWE): A Validation Study From Simulations to Experiments. *IEEE Trans. Biomed. Eng.* **2023**, *70*, 1758–1767. [CrossRef] [PubMed]

187. Almeida, T.W.J.; Sampaio, D.R.T.; Bruno, A.C.; Pavan, T.Z.; Carneiro, A.A.O. Comparison between shear wave dispersion magneto motive ultrasound and transient elastography for measuring tissue-mimicking phantom viscoelasticity. *IEEE Trans. Ultrason. Ferroelectr. Freq. Control* **2015**, *62*, 2138–2145. [CrossRef]
188. Pavan, T.Z.; Sampaio, D.R.T.; Carneiro, A.A.O.; Covas, D.T. Ultrasound-based transient elastography using a magnetic excitation. In Proceedings of the 2012 IEEE International Ultrasonics Symposium (IUS), Dresden, Germany, 7–10 October 2012. [CrossRef]
189. Deffieux, T.; Gennisson, J.L.; Bercoff, J.; Tanter, M. On the effects of reflected waves in transient shear wave elastography. *IEEE Trans. Ultrason. Ferroelectr. Freq. Control* **2011**, *58*, 2032–2035. [CrossRef]
190. Zhang, H.; Guo, Y.; Zhou, Y.; Zhu, H.; Wu, P.; Wang, K.; Ruan, L.; Wan, M.; Insana, M.F. Fluidity and elasticity form a concise set of viscoelastic biomarkers for breast cancer diagnosis based on Kelvin–Voigt fractional derivative modeling. *Biomech. Model. Mechanobiol.* **2020**, *19*, 2163–2177. [CrossRef]
191. Mierke, C.T. Viscoelasticity Acts as a Marker for Tumor Extracellular Matrix Characteristics. *Front. Cell Dev. Biol.* **2021**, *9*, 785138. [CrossRef]
192. Xie, Y.; Wang, M.; Cheng, M.; Gao, Z.; Wang, G. The viscoelastic behaviors of several kinds of cancer cells and normal cells. *J. Mech. Behav. Biomed. Mater.* **2019**, *91*, 54–58. [CrossRef] [PubMed]
193. Margueritat, J.; Virgone-Carlotta, A.; Monnier, S.; Delanoë-Ayari, H.; Mertani, H.C.; Berthelot, A.; Martinet, Q.; Dagany, X.; Rivière, C.; Rieu, J.P.; et al. High-Frequency Mechanical Properties of Tumors Measured by Brillouin Light Scattering. *Phys. Rev. Lett.* **2019**, *122*, 018101. [CrossRef] [PubMed]
194. Bacou, M.; Sjostrand, S.; Adam, G.; Kaczmarek, K.; Thomson, A.; Jansson, T. Pre-clinical development of contrast-enhanced magneto-motive ultrasound imaging of lymph nodes. In Proceedings of the 2022 IEEE International Ultrasonics Symposium (IUS), Venice, Italy, 10–13 October 2022. [CrossRef]
195. Jansson, T.; Jansson, L.; Mousavi, A.; Persson, L.; Angenete, E. Detection of magnetomotive ultrasound signals from human tissue. *Nanomed. Nanotechnol. Biol. Med.* **2023**, *47*, 102621. [CrossRef] [PubMed]
196. Axelsson, U.; Bäckström, S.; Mousavi, A.; Persson, L. Evaluation of Iron Oxide Nanoparticles for Lymph Node Detection with Magnetomotive Ultrasound—A Pilot Study in Rats. *bioRxiv* **2024**. [CrossRef]
197. Huber, C.M.; Heim, C.; Li, J.; Ermert, H.; Rupitsch, S.J.; Ulmann, l.; Lyer, S. Magnetomotive Displacement of Magnetic Nanoparticles in Different Tissue Phantoms. *Curr. Dir. Biomed. Eng.* **2024**, *10*, 324–327. [CrossRef]
198. Sjöstrand, S.; Bacou, M.; Kaczmarek, K.; Evertsson, M.; Svensson, I.K.; Thomson, A.J.; Farrington, S.M.; Moug, S.J.; Jansson, T.; Moran, C.M.; et al. Modelling of magnetic microbubbles to evaluate contrast enhanced magnetomotive ultrasound in lymph nodes—A pre-clinical study. *Br. J. Radiol.* **2022**, *95*, 20211128. [CrossRef]
199. Reniaud, J.; Evertsson, M.; Andersson, R.; Jansson, T. Increased Displacement in Magnetomotive Ultrasound Imaging by Adding a Homogeneous Magnetic Field. In Proceedings of the 2022 IEEE International Ultrasonics Symposium (IUS), Venice, Italy, 10–13 October 2022. [CrossRef]
200. Levy, B.E.; Oldenburg, A.L. Elastometry of clot phantoms via magnetomotive ultrasound-based resonant acoustic spectroscopy. *Phys. Med. Biol.* **2022**, *67*, 155010. [CrossRef]
201. Mousavi, A.; Reniaud, J.; Santesson, M.; Persson, L.; Jansson, T. Design of a Phantom Mimicking Rectal Lymph Nodes for Magnetomotive Ultrasound. *Ultrasound Med. Biol.* **2025**, *51*, 77–84. [CrossRef]
202. Nyakunu, J.; Piatnichouk, C.T.; Russell, H.C.; van Duijnhoven, N.J.; Levy, B.E. A finite element analysis model for magnetomotive ultrasound elastometry magnet design with experimental validation. *Biomed. Phys. Eng. Express* **2025**, *11*, 025048. [CrossRef]
203. Uliana, J.H.; Sampaio, D.R.T.; Sanches, A.F.; Pavan, T.Z.; Carneiro, A.A.D.O. MUSA-WAVE: A Software Platform for Magnetomotive Ultrasound and Shear Wave Analysis. In Proceedings of the 2024 IEEE UFFC Latin America Ultrasonics Symposium (LAUS), Montevideo, Uruguay, 8–10 May 2024; pp. 7–10. [CrossRef]
204. Heim, C.; Hubber, C.M.; Ermert, H.; Ullmann, I.; Saleem, T.; Lyer, S.; Rupitsch, S.J. D1.4—Modelling and Construction of Complex Shaped Polyvinyl Alcohol based Ultrasound Phantoms for Inverse Magnetomotive Ultrasound Imaging. In Proceedings of the 22nd GMA/ITG-Fachtagung Sensoren und Messsysteme, Nürnberg, Germany, 11–12 June 2024; pp. 313–318. [CrossRef]
205. Uliana, J.H.; Sampaio, D.R.T.; Carneiro, A.A.O.; Pavan, T.Z. Photoacoustic-based thermal image formation and optimization using an evolutionary genetic algorithm. *Res. Biomed. Eng.* **2018**, *34*, 147–156. [CrossRef]
206. Welch, A.J.; Van Gemert, M.J.C. Optical-thermal response of laser-irradiated tissue. In *Optical-Thermal Response of Laser-Irradiated Tissue*; Springer: New York, NY, USA, 2011.
207. Xing, L.; Wang, R.; Ha, Y.; Li, Z. Absorption characteristics and solar thermal conversion of Fe_3O_4@Au core/shell nanoparticles for a direct-absorption solar collector. *Renew. Energy* **2023**, *216*, 119120. [CrossRef]
208. Li, J.; Arnal, B.; Wei, C.W.; Shang, J.; Nguyen, T.M.; O'Donnell, M.; Gao, X. Magneto-optical nanoparticles for cyclic magnetomotive photoacoustic imaging. *ACS Nano* **2015**, *9*, 1964–1976. [CrossRef] [PubMed]
209. Walter, A.; Paul-Gilloteaux, P.; Plochberger, B.; Sefc, L.; Verkade, P.; Mannheim, J.G.; Slezak, P.; Unterhuber, A.; Marchetti-Deschmann, M.; Ogris, M.; et al. Correlated Multimodal Imaging in Life Sciences: Expanding the Biomedical Horizon. *Front. Phys.* **2020**, *8*, 47. [CrossRef]

210. Morato, Y.L.; Marciello, M.; Chamizo, L.L.; Paredes, K.O.; Filice, M. Hybrid magnetic nanoparticles for multimodal molecular imaging of cancer. In *Magnetic Nanoparticle-Based Hybrid Materials: Fundamentals and Applications*; Woodhead Publishing: Sawston, UK, 2021. [CrossRef]
211. Jin, Y.; Jia, C.; Huang, S.W.; O'Donnell, M.; Gao, X. Multifunctional nanoparticles as coupled contrast agents. *Nat. Commun.* **2010**, *1*, 41. [CrossRef]
212. Qu, M.; Mallidi, S.; Mehrmohammadi, M.; Truby, R.; Homan, K.; Joshi, P.; Chen, Y.S.; Sokolov, K.; Emelianov, S. Magneto-photo-acoustic imaging. *Biomed. Opt. Express* **2011**, *2*, 385–396. [CrossRef]
213. Cao, Y.; Chen, Y.; Yu, T.; Guo, Y.; Liu, F.; Yao, Y.; Li, P.; Wang, D.; Wang, Z.; Chen, Y.; et al. Drug release from phase-changeable nanodroplets triggered by low-intensity focused ultrasound. *Theranostics* **2018**, *8*, 1327–1339. [CrossRef]
214. Moradi Kashkooli, F.; Souri, M.; Tavakkoli, J.; CKolios, M. A spatiotemporal computational model of focused ultrasound heat-induced nano-sized drug delivery system in solid tumors. *Drug Deliv.* **2023**, *30*, 2219871. [CrossRef]
215. Luo, Z.; Jin, K.; Pang, Q.; Shen, S.; Yan, Z.; Jiang, T.; Zhu, X.; Yu, L.; Pang, Z.; Jiang, X. On-Demand Drug Release from Dual-Targeting Small Nanoparticles Triggered by High-Intensity Focused Ultrasound Enhanced Glioblastoma-Targeting Therapy. *ACS Appl. Mater Interfaces* **2017**, *9*, 31612–31625. [CrossRef]
216. Józefczak, A.; Kaczmarek, K.; Bielas, R. Magnetic mediators for ultrasound theranostics. *Theranostics* **2021**, *11*, 10091–10113. [CrossRef]
217. Tang, H.; Guo, Y.; Peng, L.; Fang, H.; Wang, Z.; Zheng, Y.; Ran, H.; Chen, Y. In Vivo Targeted, Responsive, and Synergistic Cancer Nanotheranostics by Magnetic Resonance Imaging-Guided Synergistic High-Intensity Focused Ultrasound Ablation and Chemotherapy. *ACS Appl. Mater. Interfaces* **2018**, *10*, 15428–15441. [CrossRef]
218. Jia, L.; Li, X.; Liu, H.; Xia, J.; Shi, X.; Shen, M. Ultrasound-enhanced precision tumor theranostics using cell membrane-coated and pH-responsive nanoclusters assembled from ultrasmall iron oxide nanoparticles. *Nano Today* **2021**, *36*, 101022. [CrossRef]
219. Rapoport, N.Y.; Christensen, D.A.; Fain, H.D.; Barrows, L.; Gao, Z. Ultrasound-triggered drug targeting of tumors in vitro and in vivo. *Ultrasonics* **2004**, *42*, 943–950. [CrossRef]
220. Kaczmarek, K.; Hornowski, T.; Dobosz, B.; Józefczak, A. Influence of magnetic nanoparticles on the focused ultrasound hyperthermia. *Materials* **2018**, *11*, 1607. [CrossRef] [PubMed]
221. Lundy, D.J.; Nguyễn, H.; Hsieh, P.C.H. Emerging nano-carrier strategies for brain tumor drug delivery and considerations for clinical translation. *Pharmaceutics* **2021**, *13*, 1193. [CrossRef] [PubMed]
222. Izadifar, Z.; Izadifar, Z.; Chapman, D.; Babyn, P. An introduction to high intensity focused ultrasound: Systematic review on principles, devices, and clinical applications. *J. Clin. Med.* **2020**, *9*, 460. [CrossRef]
223. Song, X.; Qian, H.; Yu, Y. Nanoparticles Mediated the Diagnosis and Therapy of Glioblastoma: Bypass or Cross the Blood–Brain Barrier. *Small* **2023**, *19*, e2302613. [CrossRef]
224. Yang, F.Y.; Teng, M.C.; Lu, M.; Liang, H.F.; Lee, Y.R.; Yen, C.C.; Liang, M.-L.; Wong, T.-T. Treating glioblastoma multiforme with selective high-dose liposomal doxorubicin chemotherapy induced by repeated focused ultrasound. *Int. J. Nanomed.* **2012**, *7*, 965–974. [CrossRef]
225. Huber, C.M.; Hageroth, L.; Dorsch, N.; Ringel, J.; Ermert, H.; Vossiek, M.; Rupitsch, S.J.; Ullmann, I.; Lyer, S. Dual-Modality Ultrasound Imaging of SPIONs Distribution via Combined Magnetomotive and Passive Cavitation Imaging. *Sensors* **2025**, *25*, 7171. [CrossRef]
226. Zhang, T.; Zheng, Q.; Xie, C.; Fan, G.; Wang, Y.; Wu, Y.; Fu, Y.; Huang, J.; Craig, D.Q.M.; Cai, X.; et al. Integration of Silica Nanorattles with Manganese-Doped In_2S_3/InOOH to Enable Ultrasound-Mediated Tumor Theranostics. *ACS Appl. Mater. Interfaces* **2023**, *15*, 4883–4894. [CrossRef]
227. Dennahy, I.S.; Han, Z.; Maccuaig, W.M.; Chalfant, H.M.; Condacse, A.; Hagood, J.M.; Claros-Sorto, J.C.; Razaq, W.; Holter-Chakrabarty, J.; Squires, R.; et al. Nanotheranostics for Image-Guided Cancer Treatment. *Pharmaceutics* **2022**, *14*, 917. [CrossRef]
228. Ivkov, R. Magnetic nanoparticle hyperthermia: A new frontier in biology and medicine? *Int. J. Hyperth.* **2013**, *29*, 703–705. [CrossRef] [PubMed]
229. Kozissnik, B.; Bohorquez, A.C.; Dobson, J.; Rinaldi, C. Magnetic fluid hyperthermia: Advances, challenges, and opportunity. *Int. J. Hyperth.* **2013**, *29*, 706–714. [CrossRef]
230. Carrey, J.; Mehdaoui, B.; Respaud, M. Simple models for dynamic hysteresis loop calculations of magnetic single-domain nanoparticles: Application to magnetic hyperthermia optimization. *J. Appl. Phys.* **2011**, *109*, 083921. [CrossRef]
231. Deatsch, A.E.; Evans, E.E. Heating efficiency in magnetic nanoparticle hyperthermia. *J. Magn. Magn. Mater.* **2014**, *354*, 163–172. [CrossRef]
232. Dennis, C.L.; Ivkov, R. Physics of heat generation using magnetic nanoparticles for hyperthermia. *Int. J. Hyperth.* **2013**, *29*, 715–729. [CrossRef]
233. Gilchrist, R.K.; Medal, R.; Shorey, W.D.; Hanselman, R.C.; Parrott, J.C.; Taylor, C.B. Selective inductive heating of lymph nodes. *Ann. Surg.* **1957**, *146*, 596–606. [CrossRef] [PubMed]

234. Jordan, A.; Wust, P.; Fähling, H.; John, W.; Hinz, A.; Felix, R. Inductive heating of ferrimagnetic particles and magnetic fluids: Physical evaluation of their potential for hyperthermia. *Int. J. Hyperth.* **2009**, *9*, 51–68. [CrossRef]
235. Andrä, W.; D'Ambly, C.G.; Hergt, R.; Hilger, I.; Kaiser, W.A. Temperature distribution as function of time around a small spherical heat source of local magnetic hyperthermia. *J. Magn. Magn. Mater.* **1999**, *194*, 197–203. [CrossRef]
236. Mahmoudi, K.; Bouras, A.; Bozec, D.; Ivkov, R.; Hadjipanayis, C. Magnetic hyperthermia therapy for the treatment of glioblastoma: A review of the therapy's history, efficacy and application in humans. *Int. J. Hyperth.* **2018**, *34*, 1316–1328. [CrossRef]
237. Maier-Hauff, K.; Ulrich, F.; Nestler, D.; Niehoff, H.; Wust, P.; Thiesen, B.; Orawa, H.; Budach, V.; Jordan, A. Efficacy and safety of intratumoral thermotherapy using magnetic iron-oxide nanoparticles combined with external beam radiotherapy on patients with recurrent glioblastoma multiforme. *J. Neurooncol.* **2011**, *103*, 317–324. [CrossRef] [PubMed]
238. Dennis, C.L.; Jackson, A.J.; Borchers, J.A.; Hoopes, P.J.; Strawbridge, R.; Foreman, A.R.; van Lierop, J.; Grüttner, C.; Ivkov, R. Nearly complete regression of tumors via collective behavior of magnetic nanoparticles in hyperthermia. *Nanotechnology* **2009**, *20*, 395103. [CrossRef]
239. Jordan, A.; Scholz, R.; Maier-Hauff, K.; Johannsen, M.; Wust, P.; Nadobny, J.; Schirra, H.; Schmidt, H.; Deger, S.; Loening, S.; et al. Presentation of a new magnetic field therapy system for the treatment of human solid tumors with magnetic fluid hyperthermia. *J. Magn. Magn. Mater.* **2001**, *225*, 118–126. [CrossRef]
240. Gneveckow, U.; Jordan, A.; Scholz, R.; Brüß, V.; Waldöfner, N.; Ricke, J.; Feussner, A.; Hildebrandt, B.; Rau, B.; Wust, P. Description and characterization of the novel hyperthermia- and thermoablation-system MFH®300F for clinical magnetic fluid hyperthermia. *Med. Phys.* **2004**, *31*, 1444–1451. [CrossRef]
241. Johannsen, M.; Gneveckow, U.; Taymoorian, K.; Thiesen, B.; Waldöfner, N.; Scholz, R.; Jung, K.; Jordan, A.; Wust, P.; Loening, A.S. Morbidity and quality of life during thermotherapy using magnetic nanoparticles in locally recurrent prostate cancer: Results of a prospective phase I trial. *Int. J. Hyperth.* **2007**, *23*, 315–323. [CrossRef]
242. Thiesen, B.; Jordan, A. Clinical applications of magnetic nanoparticles for hyperthermia. *Int. J. Hyperth.* **2008**, *24*, 467–474. [CrossRef]
243. Włodarczyk, A.; Gorgoń, S.; Radoń, A.; Bajdak-Rusinek, K. Magnetite Nanoparticles in Magnetic Hyperthermia and Cancer Therapies: Challenges and Perspectives. *Nanomaterials* **2022**, *12*, 1807. [CrossRef]
244. Zhang, Y.; Gao, X.; Yan, B.; Wen, N.; Lee, W.S.V.; Liang, X.J.; Liu, X. Enhancement of CD8+ T-Cell-Mediated Tumor Immunotherapy via Magnetic Hyperthermia. *ChemMedChem* **2022**, *17*, e202100656. [CrossRef]
245. Szwed, M.; Marczak, A. Application of Nanoparticles for Magnetic Hyperthermia for Cancer Treatment—The Current State of Knowledge. *Cancers* **2024**, *16*, 1156. [CrossRef]
246. Vilas-Boas, V.; Carvalho, F.; Espiña, B. Magnetic hyperthermia for cancer treatment: Main parameters affecting the outcome of in vitro and in vivo studies. *Molecules* **2020**, *25*, 2874. [CrossRef]
247. Chang, M.; Hou, Z.; Wang, M.; Li, C.; Lin, J. Recent Advances in Hyperthermia Therapy-Based Synergistic Immunotherapy. *Adv. Mater.* **2021**, *33*, e2004788. [CrossRef] [PubMed]
248. Atkinson, W.J.; Brezovich, I.A.; Chakraborty, D.P. Usable Frequencies in Hyperthermia with Thermal Seeds. *IEEE Trans. Biomed Eng.* **1984**, *BME-31*, 70–75. [CrossRef]
249. Nigoghossian, K.; Bouvet, B.; Félix, G.; Sene, S.; Costa, L.; Milhet, P.E.; Carneiro Neto, A.N.; Carlos, L.D.; Oliviero, E.; Guari, Y.; et al. Magneto-Induced Hyperthermia and Temperature Detection in Single Iron Oxide Core-Silica/Tb^{3+}/Eu^{3+}(Acac) Shell Nano-Objects. *Nanomaterials* **2022**, *12*, 3109. [CrossRef]
250. Ximendes, E.; Marin, R.; Shen, Y.; Ruiz, D.; Gómez-Cerezo, D.; Rodríguez-Sevilla, P.; Lifante, J.; Viveros-Méndez, P.X.; Gámez, F.; García-Soriano, D.; et al. Infrared-Emitting Multimodal Nanostructures for Controlled In Vivo Magnetic Hyperthermia. *Adv. Mater.* **2021**, *33*, 2100077. [CrossRef] [PubMed]
251. Capistrano, G.; Sousa-Junior, A.A.; Silva, R.A.; Mello-Andrade, F.; Cintra, E.R.; Santos, S.; Nunes, A.D.; Lima, R.M.; Zufelato, N.; Oliveira, A.S.; et al. IR-780-Albumin-Based Nanocarriers Promote Tumor Regression Not only from Phototherapy but Also by a Nonirradiation Mechanism. *ACS Biomater. Sci. Eng.* **2020**, *6*, 4523–4538. [CrossRef]
252. Pearce, J.A. Comparative analysis of mathematical models of cell death and thermal damage processes. *Int. J. Hyperth.* **2013**, *29*, 262–280. [CrossRef] [PubMed]
253. Hilger, I.; Kaiser, W.A. Iron oxide-based nanostructures for MRI and magnetic hyperthermia. *Nanomedicine* **2012**, *7*, 1443–1459. [CrossRef] [PubMed]
254. Healy, S.; Bakuzis, A.F.; Goodwill, P.W.; Attaluri, A.; Bulte, J.W.M.; Ivkov, R. Clinical magnetic hyperthermia requires integrated magnetic particle imaging. *Wiley Interdiscip. Rev. Nanomed. Nanobiotechnol.* **2022**, *14*, e1779. [CrossRef]
255. Chandrasekharan, P.; Tay, Z.W.; Hensley, D.; Zhou, X.Y.; Fung, B.K.L.; Colson, C.; Lu, Y.; Fellows, D.B.; Huynh, Q.; Saayujya, C.; et al. Using magnetic particle imaging systems to localize and guide magnetic hyperthermia treatment: Tracers, hardware, and future medical applications. *Theranostics* **2020**, *10*, 2965–2981. [CrossRef]
256. Yang, J.; Shi, Z.; Liu, R.; Wu, Y.; Zhang, X. Combined-therapeutic strategies synergistically potentiate glioblastoma multiforme treatment via nanotechnology. *Theranostics* **2020**, *10*, 3223–3239. [CrossRef] [PubMed]

257. Wilhelm, S.; Tavares, A.J.; Dai, Q.; Ohta, S.; Audet, J.; Dvorak, H.F.; Chan, W.C. Analysis of nanoparticle delivery to tumours. *Nat. Rev. Mater.* **2016**, *1*, 16014. [CrossRef]
258. Pucci, C.; De Pasquale, D.; Marino, A.; Martinelli, C.; Lauciello, S.; Ciofani, G. Hybrid Magnetic Nanovectors Promote Selective Glioblastoma Cell Death through a Combined Effect of Lysosomal Membrane Permeabilization and Chemotherapy. *ACS Appl. Mater. Interfaces* **2020**, *12*, 29037–29055. [CrossRef] [PubMed]
259. Wang, J.; Zhao, H.; Zhou, Z.; Zhou, P.; Yan, Y.; Wang, M.; Yang, H.; Zhang, Y.; Yang, S. MR/SPECT Imaging Guided Photothermal Therapy of Tumor-Targeting Fe@Fe_3O_4 Nanoparticles in Vivo with Low Mononuclear Phagocyte Uptake. *ACS Appl. Mater. Interfaces* **2016**, *8*, 19872–19882. [CrossRef]
260. Senturk, F.; Cakmak, S.; Kocum, I.C.; Gumusderelioglu, M.; Ozturk, G.G. GRGDS-conjugated and curcumin-loaded magnetic polymeric nanoparticles for the hyperthermia treatment of glioblastoma cells. *Colloids Surf. A Physicochem. Eng. Asp.* **2021**, *622*, 126648. [CrossRef]
261. Piao, D.; Towner, R.A.; Smith, N.; Chen, W.R. Magnetothermoacoustics from magnetic nanoparticles by short bursting or frequency chirped alternating magnetic field: A theoretical feasibility analysis. *Med. Phys.* **2013**, *40*, 063301. [CrossRef]
262. Liu, H.; Li, Y.; Liu, G. Thermoacoustic concentration imaging of magnetic nanoparticles under single-pulse magnetic fields. *AIP Adv.* **2022**, *12*, 115217. [CrossRef]
263. Liu, H.; Li, Y.; Liu, G. Thermoacoustic tomography from magnetic nanoparticles by single-pulse magnetic field. *Med. Phys.* **2022**, *49*, 521–531. [CrossRef]
264. Feng, X.; Gao, F.; Zheng, Y. Modulatable magnetically mediated thermoacoustic imaging with magnetic nanoparticles. *Appl. Phys. Lett.* **2015**, *106*, 153702. [CrossRef]
265. Feng, X.; Gao, F.; Kishor, R.; Zheng, Y. Coexisting and mixing phenomena of thermoacoustic and magnetoacoustic waves in water. *Sci. Rep.* **2015**, *5*, 11489. [CrossRef]
266. Oldenburg, A.L.; Crecea, V.; Rinne, S.A.; Boppart, S.A. Phase-resolved magnetomotive OCT for imaging nanomolar concentrations of magnetic nanoparticles in tissues. *Opt. Express* **2008**, *16*, 11525–11539. [CrossRef] [PubMed]
267. Huang, P.C.; Chaney, E.J.; Aksamitiene, E.; Barkalifa, R.; Spillman, D.R.; Bogan, B.J.; Boppart, A.S. Biomechanical sensing of in vivo magnetic nanoparticle hyperthermia-treated melanoma using magnetomotive optical coherence elastography. *Theranostics* **2021**, *11*, 5620–5633. [CrossRef] [PubMed]
268. Mehrmohammadi, M.; Yoon, K.Y.; Qu, M.; Johnston, K.P.; Emelianov, S.Y. Enhanced pulsed magneto-motive ultrasound imaging using superparamagnetic nanoclusters. *Nanotechnology* **2011**, *22*, 045502. [CrossRef] [PubMed]

Disclaimer/Publisher's Note: The statements, opinions and data contained in all publications are solely those of the individual author(s) and contributor(s) and not of MDPI and/or the editor(s). MDPI and/or the editor(s) disclaim responsibility for any injury to people or property resulting from any ideas, methods, instructions or products referred to in the content.